International Journal of Bioprinting

RESEARCH ARTICLE

Laser bioprinting of human iPSC-derived neural stem cells and neurons: Effect on cell survival, multipotency, differentiation, and neuronal activity

Lothar Koch[1,2†*], Andrea Deiwick[1,2†], Jordi Soriano[3,4†], Boris Chichkov[1,2]

[1]Institut für Quantenoptik, Leibniz Universität Hannover, 30167 Hannover, Germany

[2]NIFE—Niedersächsisches Zentrum für Biomedizintechnik, Implantatforschung und Entwicklung, 30625 Hannover, Germany

[3]Departament de Física de la Matèria Condensada, Universitat de Barcelona, 08028 Barcelona, Spain

[4]Universitat de Barcelona Institute of Complex Systems (UBICS), Barcelona, Spain

Abstract

Generation of human neuronal networks by three-dimensional (3D) bioprinting is promising for drug testing and hopefully will allow for the understanding of cellular mechanisms in brain tissue. The application of neural cells derived from human induced-pluripotent stem cells (hiPSCs) is an obvious choice, since hiPSCs provide access to cells unlimited in number and cell types that could be generated by differentiation. The questions in this regard include which neuronal differentiation stage is optimal for printing of such networks, and to what extent the addition of other cell types, especially astrocytes, supports network formation. These aspects are the focus of the present study, in which we applied a laser-based bioprinting technique and compared hiPSC-derived neural stem cells (NSCs) with neuronal differentiated NSCs, with and without the inclusion of co-printed astrocytes. In this study, we investigated in detail the effects of cell types, printed droplet size, and duration of differentiation before and after printing on viability, as well as proliferation, stemness, differentiation potential, formation of dendritic extensions and synapses, and functionality of the generated neuronal networks. We found a significant dependence of cell viability after dissociation on differentiation stage, but no impact of the printing process. Moreover, we observed a dependence of the abundance of neuronal dendrites on droplet size, a marked difference between printed cells and normal cell culture in terms of further differentiation of the cells, especially differentiation into astrocytes, as well as neuronal network formation and activity. Notably, there was a clear effect of admixed astrocytes on NSCs but not on neurons.

Keywords: Bioprinting; Laser; Neurons; Neural stem cells; Synapse; Neuronal networks; Collective neuronal activity

[†]These authors contributed equally to this work.

***Corresponding author:**
Lothar Koch
(koch@iqo.uni-hannover.de)

Citation: Koch L, Deiwick A, Soriano J, *et al*., 2023, Laser bioprinting of human iPSC-derived neural stem cells and neurons: Effect on cell survival, multipotency, differentiation, and neuronal activity. *Int J Bioprint*. 9(2): 672. https://doi.org/10.18063/ijb.v9i2.672

Received: September 24, 2022
Accepted: October 13, 2022
Published Online: January 18, 2023

1. Introduction

Three-dimensional (3D)-bioprinted organ models are promising alternatives for testing of pharmaceuticals, chemicals, or cosmetics on animals or simple cell cultures. They could also provide better understanding into cellular mechanisms of specific diseases and, by applying patient-derived cells, could enable generation of patient-specific disease models for personalized medicine.

For neural disorders, like epilepsy, schizophrenia, bipolar disorder, Parkinson's disease, or Alzheimer's disease, which affect more than one out of seven people[1], different cell-based brain models are being investigated[2], which usually are based on simple cell culture systems, 3D cell cultures in hydrogels, cell-seeded scaffolds, or cell aggregates (organoids, spheroids)[3-11]. 3D bioprinting could advance such models toward 3D brain tissue constructs with a higher level of complexity and functionality.

For personalized brain models, patient-derived neural cells can be generated by reprogramming cells from blood or skin to human induced-pluripotent stem cells (hiPSCs)[12,13] and differentiating them to multipotent neural stem cells (NSCs)[14] and further down the neuronal differentiation pathway. Thus, different types of required cells like neurons, glial cells such as astrocytes or oligodendrocytes, and endothelial cells can be generated[15-17] and 3D-bioprinted with determined brain-tissue-like patterning.

Published studies demonstrating the printing of neural cells applied mouse, rat, or human cells. These were primary neurons (rat[18-24] and mouse[25]), primary neural stem and progenitor cells or neural stem cell lines (mouse[26,27]), neural progenitor cell lines (human[18]), or neurons and neural stem and progenitor cells derived from iPSCs (mouse[28] and human[28-33]). Gu et al. printed hiPSCs and differentiated them to neurons post-printing[34] and also used immortalized human neural progenitor cells[35]. Aside from neural stem cells and neurons, glial cells such as astrocytes (rat[19]), oligodendrocytes (mouse iPSC-derived[28]), and Schwann cells (rat[36-40], porcine[41]) were printed.

For different printing technologies and bioinks, these studies demonstrated printing of neural cells in controlled patterns, achieving high viability post-printing, maintenance of neuronal phenotypes, morphology, and basic electrophysiological functions[18,21-23,25,29,30,32,37-39,41]; neurite outgrowth, formation of synaptic contacts and networks, as well as spontaneous and stimulated neuronal activity were shown[19,20,22,24,25,28,32,35].

For these printing experiments, mostly extrusion and inkjet printers were used. Since their nozzle-based printing techniques differ fundamentally from nozzle-free laser-based bioprinting applied in this study, results on potential cell impairment are not directly transferable. We prefer laser-based bioprinting due to its versatility, to print droplets of cell-containing sols (non-gelled precursors of gels) with low or high cell density (>10^8 mL^{-1}) and low or high viscosity (1 mPa·s up to more than 1 Pa·s for printing of cells) with volumes from a few picoliters up to the nanoliter range. For instance, Chrisey et al. published two studies of printing rat neuronal cells with laser-based bioprinting, applying a neuronal blastoma cell line[42] and dorsal root ganglion neurons[23]. They applied different biomaterials in each study and investigated cell survival after printing. To the best of our knowledge, however, a direct comparison of the behavior of different neural cell types upon laser-based bioprinting has not been explored yet, and has only been investigated to a very limited extent in studies applying other printing technologies [43,44].

Having all the different options for cells raises the following questions: (i) Which cellular differentiation stages are optimal for printing brain tissue models? (ii) For these differentiation stages, does co-printing of other cell types like glial cells support neuronal network formation? In this study, we investigated laser printing of NSCs and pre-differentiated neurons, partially together with astrocytes, which were all derived from hiPSCs.

In a previous study, we compared the application of different biomaterials for printing of hiPSCs[45] and found that the best approach was to print with a bioink composed of hyaluronic acid and cell culture medium onto a layer of Matrigel™. Given these findings, we used the same biomaterials in our experiments on hiPSC-derived NSCs presented here. Matrigel™ was also used by other groups[28,30,42] for printing of neural cells.

Our present study includes assessment of post-printing viability and proliferation of NSCs and pre-differentiated neurons (all derived from hiPSCs), maintenance of NSCs stemness, differentiation of printed NSCs toward neurons and glia cells, formation of dendrites and synapses by printed NSCs during differentiation, as well as statistical evaluation of the functionality of neuronal networks formed by printed post-differentiated NSCs and neurons. We used fluorescence calcium imaging to monitor and evaluate the behavior of the printed neuronal networks. Thereby, the frequency and intensity of collective neuronal activity, i.e., events in which many neurons are active simultaneously, are considered a measure of the functionality of these networks.

NSCs were compared with NSCs cultivated under neuronal differentiation conditions (pre-differentiated) for 5, 10, or 20 days to identify the optimal differentiation stage for generating neuronal networks by laser printing. Furthermore, we also studied whether co-printing of astrocytes increases

or accelerates neuronal network formation. Our results show a clear effect of pre-differentiation on cell viability and behavior after printing and contrary to our expectations, a stronger effect of added astrocytes on un-differentiated NSCs than on pre-differentiated ones.

1.1. Notation

All cells used for this study were NSCs derived from hiPSCs. Some of these NSCs were differentiated to neurons or astrocytes. This produced mixtures of cells from different differentiation stages.

To avoid repetitive long descriptions for these mixtures, we use the following notation for neuronal differentiation of NSCs: For cells printed as NSCs and differentiated after printing, we use the term "post-differentiated NSCs" to distinguish them from "NSCs" that were already differentiated before printing (pre-differentiated), which we call "neurons" or, e.g., "d10 neurons" for 10 days of pre-differentiation. Additionally, we use the notation "(day A pp, diff B/C)," which reads "cells assessed A days post-printing with B days of pre-differentiation and C days of post-differentiation." For a more detailed description and rationale, see section 2.2.

2. Materials and methods

2.1. Materials

Cell culture media, supplements, and hydrogels were purchased from Fisher Scientific GmbH (Schwerte, Germany). Cell culture flasks and plates were obtained from TPP-Techno Plastic Products AG (Trasadingen, Switzerland). Chemicals and antibodies were purchased from Sigma-Aldrich (Deisenhofen, Germany), unless otherwise noted.

2.1.1. Cells

All cells used were NSCs derived from hiPSCs or differentiated from these NSCs under neuronal or astrocytic culture conditions. This produced mixtures of cells from different differentiation stages. After 10 days of neuronal differentiation, the majority of the cells showed markers of mature neurons, but there were also NSCs that were not yet differentiated. In addition, some cells did also spontaneously differentiate in a different direction. For example, a few astrocytes were also found in neuronal differentiated cell cultures.

In this study, NSCs were printed without prior differentiation, after neuronal differentiation for 5, 10, or 20 days, or after astrocytic differentiation. To avoid repetitive long descriptions, we will hereafter refer "NSCs" to as cells that have not been cultured in differentiation medium before the time of printing as NSCs, NSCs that have been in astrocytic differentiation culture as astrocytes, and NSCs that have been cultured under neuronal differentiation conditions for 5, 10, or 20 days before printing as neurons or as d10 neurons after 10 days of differentiation.

After most printing experiments, cells were cultured under neuronal differentiation conditions. While neurons were directly further kept under neuronal differentiation conditions, printed NSCs were kept under normal NSC culture conditions for 2 days after printing before the differentiation was started to enable distinction between the effects of medium change and printing. This results in the need for a distinction between differentiation before and after printing, for which we will use the terms "pre-differentiation" and "post-differentiation," and a distinction between the time since printing and the time duration of differentiation after printing, which is the same for neurons (pre-differentiated NSCs) but differs by two days for NSCs (non-pre-differentiated NSCs).

Therefore, we will use the following notations for neuronal differentiation of NSCs: For not pre-differentiated cells we will use the term '"NSCs" and "post-differentiated NSCs," when differentiated after printing. For astrocytic pre-differentiated NSCs, we use the term "astrocytes," and for neuronal pre-differentiated NSCs, we use the term "neurons," even though strictly speaking, it is a mixture of neurons, NSCs and also some astrocytes and sometimes oligodendrocytes. We call these neurons, e.g., "d10 neurons," for 10 days of pre-differentiation. Additionally, we use the notation "(day A pp, diff B/C)," which reads "cells assessed A days post-printing with B days of pre-differentiation and C days of post-differentiation."

2.1.2. Cell culture media

In the cell culture of this study, four different cell culture media were used, a plating medium to initially seed the NSCs after thawing, an expansion medium to proliferate the NSCs, a neuronal differentiation medium to stimulate the differentiation of the NSCs into neurons, and an astrocytic differentiation medium to stimulate the differentiation of the NSCs into astrocytes. Immediately after the cells were passaged or printed, medium with added RevitaCell™ was used. RevitaCell™ is a modified Rho-kinase inhibitor that promotes adhesion of neuronal cells and prevents cell death. After 1 day, the medium was replaced by medium without RevitaCell™.

2.2. Cell culture

2.2.1. Stem cell culture

hiPSC-derived NSCs (ax0011, Axol Biosciences Ltd., Cambridge, UK) were used in this study. The NSCs were thawed and cultured as instructed by the supplier. Briefly, NSCs were seeded at a density of 5×10^4 cells cm^{-2} in Neural Plating-XF Medium (Axol Biosciences) onto SureBond

(Axol Biosciences)-coated 6-well plates and cultured for 24 hours at 37°C in a 5% CO_2 environment. The plating medium was then replaced with expansion medium consisting of KnockOut™ DMEM/F-12 supplemented with 2% StemPro™ Neural Supplement, 1% Glutamax™, basic fibroblast growth factor (bFGF, 20 ng mL^{-1}; Axol Bioscience), epidermal growth factor (EGF, 20 ng mL^{-1}; Axol Bioscience), and 50 µg mL^{-1} gentamycin. For passaging, NSCs were washed once with phosphate-buffered saline (PBS) and then dissociated into single cells with Accutase™ for 5 minutes at 37°C. After gentle pipetting, the cells were collected by centrifugation at 400 ×g for 5 minutes. NSCs were seeded at a density of 5×10^4 cells cm^{-2} and cultured onto Geltrex-ESC™-coated 6-well plates in expansion medium supplemented with 1% RevitaCell™ during initial plating. Medium was fully exchanged to expansion medium without RevitaCell™ after 24 hours. NSCs were maintained in expansion medium with medium changes twice a week. NSCs from passages 3–5 were used for the cell printing experiments.

2.2.2. Neuronal differentiation

For the experiments with pre-differentiated neurons, NSCs were plated at a density of 1×10^5 cells cm^{-2} onto Geltrex-ESC™-coated plates in expansion medium supplemented with 1% RevitaCell™. Medium was changed the next day to expansion medium without further supplementation. At a confluence of 40%–60%, the expansion medium was switched to neuronal differentiation medium (Neurobasal medium, 2% B27™ Serum-Free Supplement, 1% Glutamax™, 200 µm ascorbic acid-2-phosphate, and 50 µg mL^{-1} gentamycin). Half of the medium volume was exchanged every second day.

2.2.3. Astrocytic differentiation

For the printing experiments with astrocytes, NSCs were plated at a density of 1×10^5 cells cm^{-2} onto Geltrex-ESC™-coated plates in expansion medium supplemented with 1% RevitaCell™. Medium was switched the next day to astrocyte differentiation medium (DMEM, 1% N2™ Supplement, 1% fetal bovine serum (FBS), 1% Glutamax™, and 50 µg mL^{-1} gentamycin). Medium was thereafter fully exchanged twice a week. Cells were split (1:4 ratio) at a confluence of 80%–90% by using Accutase™. Astrocytes from passages 5–7 were used for the cell printing experiments. Astrocytic differentiation was confirmed by the staining of glial fibrillary acidic protein (GFAP), a general astrocyte marker that does not require fully mature astrocytes.

2.3. Cell printing

2.3.1. Cell preparation for printing and immunostaining

For printing and immunostaining, NSCs, astrocytes and neurons after 5, 10, and 20 days pre-differentiation period, were dissociated into single cells with Accutase™ for 5 minutes at 37°C. After gentle pipetting, the cells were collected by centrifugation at 200 ×g for 5 minutes and carefully resuspended in their respective cell culture medium supplemented with 1% RevitaCell™. The majority of these cells were used for the printing experiments, and a smaller portion of the cells were analyzed with respect to their differentiation stage and composition. The latter were seeded at a cell concentration 2.5×10^4 cells cm^{-2} on Matrigel™-coated glass coverslips in their respective cell culture medium and allowed to attach for 4 hours in an incubator at 37°C in a 5% CO_2 environment.

2.3.2. Cell printing system

The printing system applied in this study was described in our previous publication[46]. Briefly, for laser printing, cells are suspended in a sol (referred to as bioink), usually consisting of several components; a sol is the non-gelled precursor of a gel. A glass slide (donor) is coated with a 60 nm thin laser-absorbing gold layer and a thicker (50–70 µm) layer of the cell containing bioink. The donor is mounted upside-down (Figure 1A) above a second glass slide (collector), which is coated with a layer of hydrogel (referred to as substrate) to provide a humid environment and to prevent printed cells from dehydration and drying out due to the extremely small droplet volumes. For some cell types, the hydrogel layer is also necessary to enable cell adhesion after printing.

For printing bioink droplets, laser pulses are focused through the donor glass slide into the absorbing layer which is evaporated in the laser focus. An expanding vapor bubble is generated, which propels the subjacent bioink downward. Due to the vapor bubble collapsing after a few microseconds, a bioink jet is formed, lasting for a few hundred microseconds[47]. The bioink deposits as a droplet on the collector substrate. Arbitrary patterns can be generated by moving laser focus and donor slide; 3D structures and tissues are printable layer-by-layer. The printed droplet volume depends on laser pulse energy and focused laser spot size, as well as on thickness and viscosity of laser-absorbing layer and bioink layer. In this study, droplet volumes in the range of 0.1–1 nL were printed. Former studies demonstrated that no heat shock was induced to the printed cells[48].

A Nd:YAG laser (DIVA II; Thales Laser, Orsay, France) with 1064 nm wavelength, approximately 10 ns pulse duration (FWHM) and 20 Hz repetition rate was used. The laser pulses were focused with a 50 mm achromatic lens into an ablation spot with a 40 µm diameter. Depending on the bioink layer thickness (approx. 60 µm) and viscosity, the laser pulse energy was set between 10 and 15 µJ, corresponding to laser fluences around 1–2 J cm^{-2}.

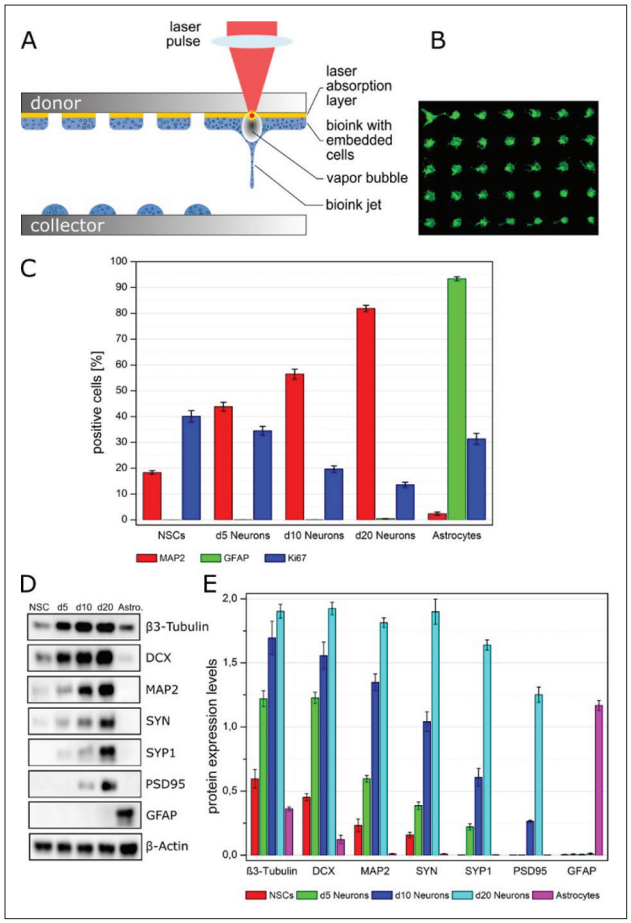

Figure 1. Printing process and cell culture homogeneity. (A) Schematic sketch of the laser-assisted bioprinting technique. (B) Example of bioprinted neuronal stem cells (NSCs): Fluorescence microscopic image of NSCs printed in a dot-pattern with a dot-to-dot distance of 600 µm, immunostained with nestin antibody (green fluorescence) for neuronal stem cells 2 days after printing. (C) Quantitative investigation of NSC's differentiation toward neurons and astrocytes (without printing); counting of positive cells for mature neuronal (MAP2), proliferation (Ki67) and astrocyte (GFAP) markers among NSCs, d5, d10, d20 neurons and astrocytes from fluorescent microscopic images; representative images are depicted in **Figure S2** (in Supplementary File). (D) Western blot (left) analysis of neuronal proteins and its quantitative representation (right) of the expression level of β3-tubulin, doublecortin (DCX), MAP2, synaptophysin (SYN), synapsin-1 (SYP1), PSD95, and GFAP of cells in NSC, d5, d10, d20 neuron and astrocyte culture. Data are normalized relative to internal standard β-actin band density.

2.3.3. Bioink preparation for printing

The preparation for printing followed the method used in our previous study with hiPSCs[45]. The following materials were used as bioinks and culture substrates: 66.67% (v/v) Corning™ Matrigel™, mixed with 33.33% (v/v) EBM-2 medium (Lonza, Basel, Switzerland), was applied as culture substrate; 1% (w/w) hyaluronic acid from *Streptococcus equi* (mol wt ~1.5–1.8 × 10^6 Da) in 0.1 M Tris-buffered saline (TBS), pH 7.4, mixed with the culture medium appropriate for the cells to be printed at a ratio of 15%–85% (v/v) was applied as bioink.

For printing, 1 or 2 million cells were suspended in 50 µl of bioink. 26 × 26 mm^2 donor glass slides were blade-coated with 50 µl bioink (74 µm layer thickness) and 23 × 23 mm^2 collector glass slides were coated with 60 µl of substrate hydrogel (113 µm layer thickness). Subsequently, droplets of bioink were printed onto the substrate layer on the collector slide in x/y-arrays of distinct dots (see Figure 1B) with 1 mm dot distance.

2.3.4. Cell handling after printing

After printing, the collector slide with hydrogel substrate and printed cells was stored submerged in cell culture medium in an incubator at 37°C in a 5% CO_2 environment. Culture medium was expansion medium with RevitaCell™ for printed NSCs and neuronal differentiation medium with RevitaCell™ for pre-differentiated neurons. The culture medium of printed NSCs was changed after 2 days to neuronal differentiation medium (without RevitaCell™).

For cell viability assay (Figure 1C and 1D), cells were printed with hyaluronic acid and culture media as bioink on Matrigel™ substrate. Non-printed cells residing on the donor glass slides (referred to as donor cells) were rinsed after printing, collected, centrifuged, resuspended in expansion or differentiation medium with RevitaCell™, and 50,000 of them (similar to the number of printed cells) were seeded on a glass slides coated with Matrigel™. Control cells were stored with culture medium in vials (while other cells were printed) and were seeded like donor cells when printing was finished.

2.4. Cell evaluation

2.4.1. Analysis of cell viability

Cell viability of printed, donor, and control cells was determined via calcein AM (2 µM, green-live cells) and ethidium-homodimer-1 (4 µM, red-dead cells) staining 24 hours after printing. The samples were analyzed by fluorescence microscopy using an AxioImager A1.m microscope (Carl Zeiss, Oberkochen, Germany) equipped with AxioCam ICc1 camera and AxioVision Rel. 4.8 software. Live/dead cells were counted from 10 fields of 3 independent experiments of printed, donor, and control cells. Percentage of viability is reported as mean with standard error of mean. Significance of differences is calculated by applying Student's unpaired two-sample *t*-test.

2.4.2. Immunostaining

For immunofluorescence analysis, cells printed in patterns as well as those prepared as described in section 2.4.1., were fixed in 4% paraformaldehyde for 30 minutes and

permeabilized with 0.3% Triton X-100/PBS. After blocking with 2% bovine serum albumin/PBS solution at 37°C for 1 hour, the cell samples were incubated with primary antibodies (see **Table S1** in Supplementary File for details) diluted in 0.3% Triton X-100/PBS overnight at 4°C. After several washing steps, the cell samples were incubated with a fluorescence-conjugated secondary antibody at an appropriate dilution (**Table S1**) for 1 hour at 37 °C. Cell nuclei were stained with Hoechst 33342.

2.4.3. Western blot analysis

NSCs, neurons and astrocytes were harvested at the indicated time points from three independent experiments. Total protein was isolated from the cells with RIPA lysis buffer containing protease and phosphatase inhibitors (25 mM Tris-HCl (pH 7.6), 150 mM NaCl, 1% Nonidet P-40, 0.1% sodium dodecyl sulfate [SDS], and 1% sodium deoxycholate). The protein concentrations of the cell lysates were determined using a BCA protein assay (Carl Roth, Karlsruhe, Germany). Ten micrograms of the total protein extract were loaded per lane on a 10% polyacrylamide resolving gel and separated by SDS-PAGE (sodium dodecyl sulfate–polyacrylamide gel electrophoresis). After electrophoresis, proteins were transferred onto polyvinylidene fluoride (PVDF) membranes (Carl Roth) by wet blotting using 20% methanol in Tris-glycine buffer. The membranes were blocked for 1 hour in a 5% nonfat milk solution in TBS with 0.1% Tween™ 20 before incubation with primary antibodies (**Table S1**) overnight at 4°C. After washing, the membranes were incubated with a horseradish peroxidase-conjugated secondary antibody (**Table S1**) for 2 hours at room temperature. The blots were developed with an enhanced chemiluminescence reagent SuperSignal West Femto Substrate (Thermo Scientific). The band densities of the immunoblots were quantified by applying the ImageJ software. The relative expressions levels of neuronal proteins were normalized to the housekeeping protein levels (β-actin) and are presented as mean values from three independent experiments.

2.5. Calcium imaging

2.5.1. Culture preparation and visualization

Neuronal cell cultures were incubated with the calcium-sensitive dye Fluo-8 AM (10 µM Biomol, Hamburg, Germany) in a neuronal differentiation medium for 40 minutes at 37°C in a 5% CO_2 environment. Cell cultures were then washed twice with prewarmed external medium (EM) consisting of 10 mM Hepes, 130 mM NaCl, 4 mM KCl, 1 mM $MgCl_2$, 2 mM $CaCl_2$, 45 mM sucrose, and 10 mM glucose. Spontaneous calcium activity was acquired upon an AxioImager A1.m microscope equipped with an AxioCm ICc1 camera and AxioVision Rel. 4.8 software.

Table 1. Grading system for rating the neuronal activity visualized by calcium imaging

Spontaneous activity	Without bursting events	With bursting events
No	0	N/A
Scarcely	2	N/A
Little	3	N/A
Some	4	8
Substantial	8	12
Widespread	12	16
Abundant	16	20
Abundant and intensive	20	24

2.5.2. Rating of neuronal activity visualized by calcium imaging

Approximately 500 videos were taken from printed samples with calcium imaging to investigate neuronal activity. Some of them were assessed in detail by statistical data analysis method described below. Additionally, the activity visualized in all videos was rated between 0 and 24 (points) with the grading of Table 1. Thereby, intermediary ratings were also given.

2.6. Calcium imaging data analysis

Fluorescence recordings were analyzed with the custom-made software NETCAL (www.itscnetcal.com)[49]. First, all frames of the fluorescence recording were averaged to generate a highly contrasted gray scale image where bright spots are active neurons. Regions of interest (ROIs) were then automatically identified as those circular-like spots with at least 5 µm in diameter. The fluorescence trace $F_i(t)$ for each ROI was then extracted and normalized as $\%DFF = 100\ (F_i(t)-F_{i\_0})\ F_{i\_0}^{-1}$, where F_{i_0} is the fluorescence trace of the neuron at rest. Sharp increases in the fluorescence trace revealed activity. The train of spikes' onset times for each ROI was extracted using the Schmitt trigger method, which accepts a sharp change in fluorescence as a spike when the fluorescence stays elevated for at least 100 ms between a lower and a higher threshold[50]. The two thresholds are necessary to prevent that camera noise or other artifacts are identified as spikes. The complete set of spiking events extended to all the neurons in the network provided the raster plots, and from which all statistical analyses were carried out. We associated all ROIs as neurons. Typically, a recording contained about 2,000 active neurons. Glial cells showed smooth fluorescence calcium transients that were automatically filtered out during data analysis.

2.6.1. Average neuronal activity

The average neuronal activity quantified the neurons' spontaneous activity and was computed by the number of

identified activity events per neuron and minute, averaged over all neurons in the network.

2.6.2. Global network activity (GNA) and distribution of burst amplitudes

It quantified the capacity of the neurons to exhibit coordinated activity and was computed by the fraction of neurons in the network that were active together without repetition in a sliding window of 2 s width and 0.5 s step. By construction, the GNA varied between 0 (no activity) and 1 (full network activation). Peaks in the GNA profile identified network bursts, i.e., neuronal coordinated activations that encompassed a significant part of the network. Since neuronal sporadic activity was abundant, a burst was deemed significant when its amplitude A_b verified $A_b > \mu_{bgnd} + 3\ SD_{bgnd}$, where μ_{bgnd} and SD_{bgnd} are the mean and standard deviation of background activity. All significant burst amplitudes A_b, across realizations and for a given experimental condition, were pooled together to build the distribution of amplitudes. These distributions were finally compared among experimental conditions to determine the tendency of a given preparation to show strong bursting.

2.6.3. Raster plots of collective activity

To prevent the abundance of neuronal sporadic activations from masking the computation of functional connectivity, the original raster plots of each realization were processed to generate new ones that contained only the neurons and corresponding activations of significantly strong network bursts. Thus, these rasters excluded all uncorrelated background activity. The goodness of such a strategy was investigated through numerical simulations in a recent study[51].

2.6.4. Functional connectivity

Causal relationships among pairs of neuronal spike trains were inferred from the raster plots of collective activity, and using a modified version of the Generalized Transfer Entropy (GTE)[52-54]. Given a pair of spike trains corresponding to neurons X and Y, an effective connection was established between X and Y whenever the information contained in X significantly increased the capacity to predict future states of Y. To evaluate the effective connectivity among all pairs of neurons, binarized time series ("1" for the presence of a spike, "0" for absence) were constructed and computed in a fast implementation of GTE run in MatLab. Instant feedback was present, and Markov Order was set as 2[52]. The actual GTE estimate was then compared with those from the joint distribution of all inputs to Y and all outputs to X, setting a connection as significant whenever the GTE estimate exceeded the mean + 1.5 standard deviations of the joint distribution. This threshold was considered optimal to capture the effective interactions among neurons during the bursting episodes, which is the key dynamic difference across experimental preparations. The GTE scores were finally set to 0 (absence of connection) or 1 (connection present), shaping directed yet unweighted connectivity matrices. For clarity of language, the term "functional" was used instead of "effective" throughout the description of results.

2.6.5. Network measures

The network characteristics of the inferred functional connectivity matrices were inferred using the "Brain Connectivity Toolbox"[55] run in Matlab. Two main measures were considered, namely the Global Efficiency G_{eff}[55,56] and the community statistic Q[55,57]. G_{eff} varies between 0 and 1 and accounts for the capacity of a neuronal circuit to exchange information as a whole. $G_{eff} \cong 0$ indicates that neurons tend to communicate locally and with few neighbors, while $G_{eff} \cong 1$ indicates that all neurons communicate among themselves across the entire network. Q varies between 0 and 1 and describes the strength of functional communities, i.e., groups of neurons that tend to be functionally more connected among themselves than with the rest of the network. For $Q \cong 0$, no structure is detected, and the entire network shapes the only community. A value of $Q \cong 0.3$ typically indicates clear communities. The extreme case of $Q = 1$ corresponds to the situation in which there are as many communities as neurons.

3. Results

Figure 1A provides a sketch of the cell printing technology, and Figure 1B shows the accuracy of our system to precisely allocate cells in predefined locations.

3.1. Change in the composition of cell cultures during differentiation

NSCs were partially differentiated to neurons for 5, 10, or 20 days, or to astrocytes before being used for printing experiments. At any point in time, there is a mixture of already differentiated cells and undifferentiated NSCs. The resulting cell composition was determined by fluorescence imaging and Western blot analysis.

Figure S1 (in Supplementary File) depicts phase contrast microscopic images of cells before dissociation for printing; while NSCs exhibited cortical rosettes, neurons increasingly formed dendritic extensions during pre-differentiation (d5, d10, d20 neurons). However, some cells with dendritic extensions could already be seen in the NSC culture, which demonstrates spontaneous differentiation of NSCs to neurons. Thus, NSC and neuron cultures were not homogeneous.

Fluorescence images with antibody staining for mature neuron marker MAP2, astrocytic marker GFAP, and

proliferation marker Ki67 combined with general cell nuclei marker Hoechst 33342 are shown in **Figure S1**; the ratios of cells positive for these markers, counted in between 12 and 18 of such images from 3 independent experiments, are presented in Figure 1C.

For neuronal differentiation, the percentage of MAP2-positive cells increased from 18.4 ± 0.7% (day 0 / NSCs) to 43.8 ± 1.7% (day 5), 56.4 ± 2.0% (day 10) and 81.9 ± 1.2% (day 20), while the percentage of GFAP-positive cells remained low (day 0: 0.01 ± 0.01%; day 5: 0.05 ± 0.02%; day 10: 0.04 ± 0.02%; day 20: 0.4 ± 0.1%). For astrocytic differentiation, the percentage of GFAP-positive cells increased from 0.01 ± 0.01% (day 0 / NSCs) to 93.4 ± 0.8% (astrocytes), while here the percentage of MAP2-positive cells decreased from 18.4 ± 0.7% (NSCs) to 2.4 ± 0.6% (astrocytes).

The percentage of cells positive for proliferation marker Ki67 decreased during neuronal differentiation from 40.1 ± 2.1% (NSCs) to 34.5 ± 1.7% (day 5), 19.7 ± 1.3% (day 10), and 13.6 ± 1.0% (day 20), while it decreased to 31.4 ± 2.1% during astrocytic differentiation. We observed astrocytes positive for GFAP and Ki67, which showed that these astrocytes were not yet fully matured. However, neurons, positive for MAP2, were not found to be positive for Ki67.

Protein expression levels of neuronal markers β3-tubulin, doublecortin, MAP2, synaptophysin, synapsin-1, PSD95, and GFAP, investigated by Western blot, are shown in Figure 1 for NSCs, d5, d10, d20 neurons and astrocytes as images (Figure 1D) as well as in a quantitative representation (Figure 1E). For the quantitative representation, all these levels were normalized by dividing by the β-actin expression level as a house-keeping protein. Except for GFAP, all these protein expression levels increase from NSCs via d5 and d10 neurons to d20 neurons. As expected, astrocytes are GFAP-positive, while all NSCs and cell cultures under neuronal differentiation are almost all GFAP-negative. Astrocytes also expressed β3-tubulin and doublecortin (weak), which is in accordance with literature[58,59].

3.2. Cell viability after printing

Figure 2A and 2B depict fluorescence microscopy images of live/dead-staining 24 hours after printing for NSCs, d5, d10, and d20 neurons with two different magnifications. Live/dead staining revealed apparent agglomeration of printed d10 and d20 neurons compared to NSCs and d5 neurons, an effect which increased with duration of pre-differentiation. Dead cells could be seen within these agglomerations in high-magnification images (Figure 2B).

Figure 2C compares the viability of printed cells, i.e., NSCs and neurons (pre-differentiated for 5, 10, and 20 days), with non-printed donor and control cells. Donor cells were put into the printing setup but were not transferred, while control cells were those that were not put into the setup but stored in a vial during the printing procedure. In general, we observed that the survival rate of printed neurons depended on duration of pre-differentiation period. Control, printed, and donor (c/p/d) cells' viability decreased with the duration of pre-differentiation. While the viability of d5 neurons (control: 89.9 ± 0.4%; printed: 93.0 ± 0.6%; donor: 91.0 ± 0.5%) was similar (no significant difference for c/p/d; see *P* values in Figure 2C) to that of NSCs (control: 91.1 ± 0.5%; printed: 94.5 ± 0.6%; donor: 89.1 ± 0.5%), the viability of d10 neurons (control: 76.5 ± 0.9%; printed: 79.1 ± 0.5%; donor: 75.3 ± 0.5%) was significantly ($P < 10^{-4}$ for c/p/d) lower and, when compared with d10 neurons, d20 neurons viability (control: 68.4 ± 0.8%; printed: 68.4 ± 1.3%; donor: 67.5 ± 1.0%) was again significantly lower ($P < 10^{-4}$ for c/p/d).

It is noticeable that the viability of printed cells was always higher or equal (d20 neurons) than that of donor or control cells. This difference was significant in five out of eight cases (three out of four cases for printed/donor and two out of four for printed/control); no significant difference could be seen for d20 neurons. We also observed significantly higher viability of control NSCs when compared with donor NSCs; however, this might have been an artifact.

3.3. Effect of cell density on formation of neuronal dendrites

When printing cell-containing droplets, the effect of droplet size and cell number per droplet on cells behavior post-printing is of interest. Figure 2D and 2E show the formation of neuronal dendrites of printed NSCs at day 7 of differentiation post-printing (day 9 pp, diff 0/7), which were printed in smaller (Figure 2D) and larger (Figure 2E) droplets with lower and higher cell number per droplet (bioink: hyaluronic acid and culture media; substrate: Matrigel™). Phase contrast images taken at day 1 post-printing illustrate different droplet sizes, while neuron-specific cytoskeletal marker β3-tubulin and Hoechst 33342 cell nuclei staining at day 7 post-printing (day 9 pp, diff 0/7) show that the number of neuronal dendrites relative to the number of neuronal cells is lower in smaller droplets and higher in larger droplets.

3.4. Proliferation and migration after printing

Figure 3A–C compare the proliferation and migration of NSCs and d20 neurons. They are shown at 2 days (NSCs only; Figure 3A) and 12 days after printing under neuronal differentiation conditions (day 12 pp, diff 0/10 for NSCs, Figure 3B; day 12 pp, diff 20/12 for neurons, Figure 3C). Panels show staining of proliferating cells (red, Ki67) alone and together with cell nuclei staining (blue, Hoechst 33342), as well as for the same cells, neuron-specific marker β3-

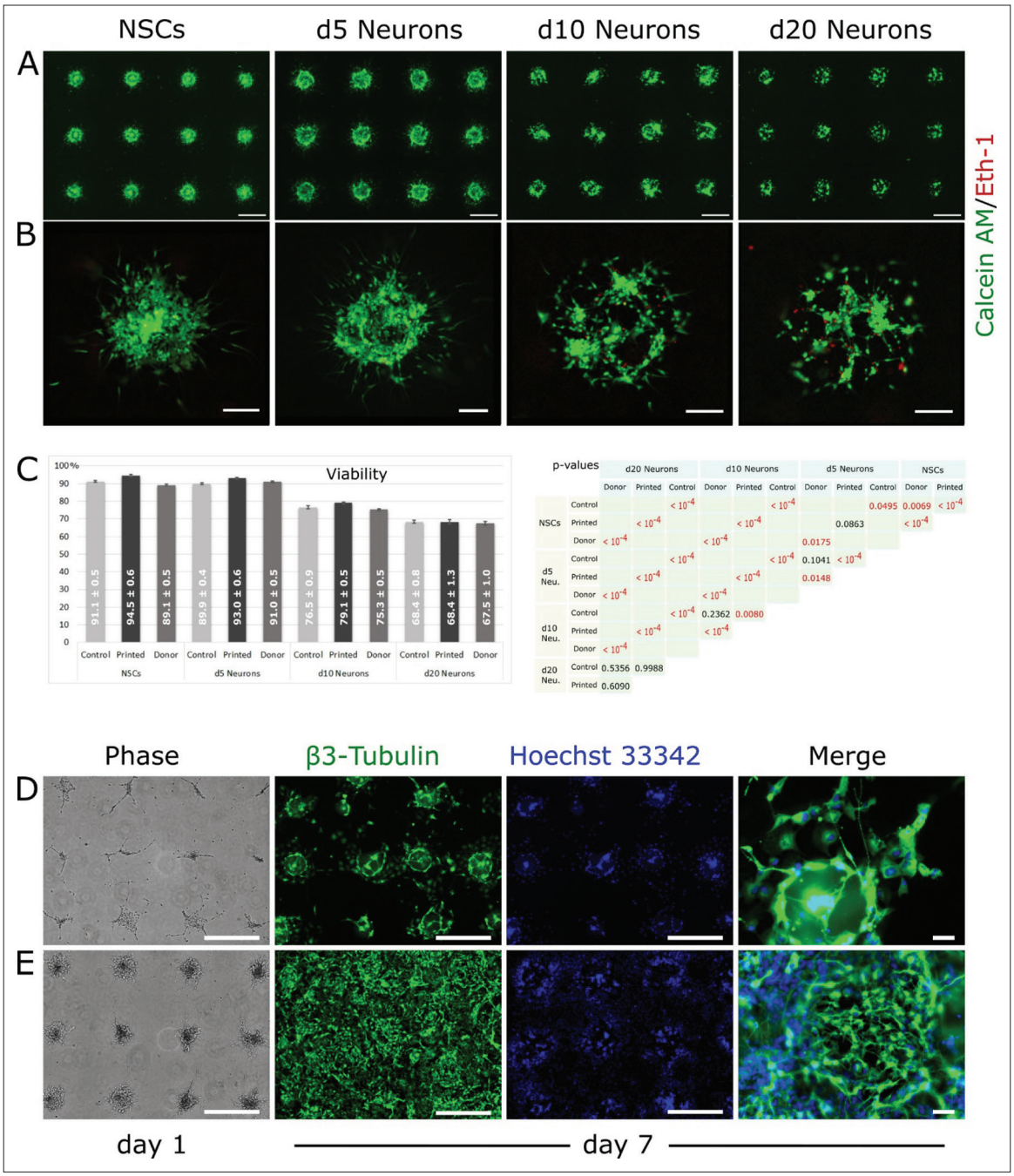

Figure 2. Cell viability, colony morphology, development of dendrites. (A and B) Fluorescent microscopic images of live/dead-staining 24 hours after printing for NSCs, d5, d10, and d20 neurons with calcein AM (green, viable cells) and ethidium homodimer-1 (red, dead cells). Live/dead staining revealed agglomeration of printed cells, increasing with duration of pre-differentiation. Dead cells could be seen within these agglomerations in high-magnification images (B). (C) Left: Viability 24 hours post-printing of printed, donor, and control cells (NSCs, d5, d10, and d20 neurons), given in percent. Control cells were not in contact to bioink or substrate, but stored in a vial, while printed and donor cells were suspended in bioink for printing. Obviously, viability decreases with duration of pre-differentiation period and viability of printed cells is mostly higher than that of donor and control cells. Right: Statistical analysis, *P* values for unpaired two-sample *t*-test. Statistical significance (highlighted in red) was determined for higher viability of printed cells when compared to control and donor cells (five out of eight cases) and for decreased viability with increasing pre-differentiation period (15 out of 18 cases). (D and E) Formation of neuronal dendrites in smaller (D) and larger (E) droplets of bioink with lower and higher number of NSCs printed on Matrigel™ substrate is depicted in phase contrast imaging 1 day post-printing and in fluorescence imaging with marker β3-tubulin and Hoechst 33342 at day 7 of post-printing differentiation. The number of neuronal dendrites relative to the number of neuronal cells is lower in smaller droplets and higher in larger droplets. Scale bars are 1 mm (D and E, except for right column), 500 μm (A) and 100 μm (all others).

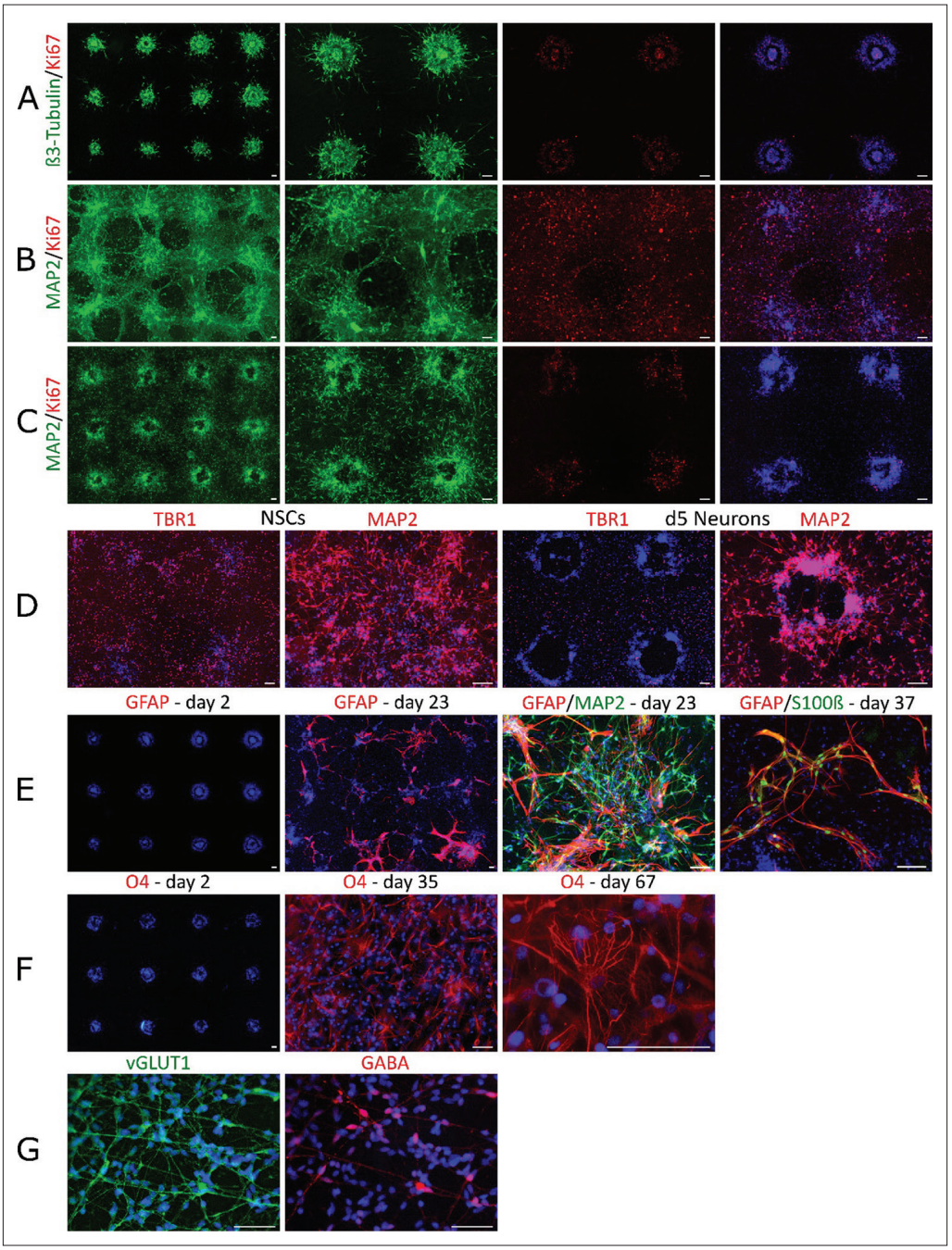

Figure 3. Proliferation and differentiation toward neurons and glial cells in printed patterns. All blue staining are general cell nuclei staining with Hoechst 33342. Scale bars: 100 µm. (A–C) Proliferation of NSCs (A and B) and d20 neurons (C) 2 days (A) and 12 days (B and C) post-printing. Ki67 staining marked nuclei of proliferating cells in red, while green staining of NSCs (β3-tubulin (A); MAP2 (B)) and d20 neurons (MAP2 (C)) stains whole cells. While both NSCs and d20 neurons migrated post-printing and proliferation of NSCs was observed everywhere, d20 neurons proliferated only at the positions of printed droplets with high cell density. (D) TBR1 and MAP2 staining of printed NSCs (left) and d5 neurons (right) 22 days after printing. The position of four printed droplets can still be seen in TBR1 panels, while there is only one droplet position depicted in MAP2 panels due to higher resolution microscopy. (E and F) NSC spontaneous differentiation to glial cells like astrocytes and oligodendrocytes under neuronal differentiation conditions. Staining with markers GFAP (red, for astrocytes), MAP2 (green), and S100B (green, for mature astrocytes) at days 2, 23, and 37 post-printing demonstrates differentiation to astrocytes under neural differentiation conditions. Staining with oligodendrocytic marker O4 (red) at days 35 and 67 of neuronal differentiation post-printing demonstrated many O4-positive cells already present on day 35, mostly pre-oligodendrocytes with simple dendritic extensions (without bifurcations) and a few immature oligodendrocytes (with a few bifurcations). On day 67, mature oligodendrocytes (with long extensions and many complex bifurcations) were also observed. (G) vGLUT1 staining (green) of glutamatergic neurons and GABA staining (red, same image section) of GABAergic neurons at day 30 of post-differentiation of printed NSCs. Most of the NSCs differentiated to glutamatergic neurons and only a smaller proportion became GABAergic neurons.

tubulin (green, Figure 3A), which already stains neurons in their earliest phases of differentiation, and mature neuronal marker MAP2 (green, Figure 3B and 3C). The left images of Figure 3A–C depict larger overviews of the printed pattern. In all cases, there was a large proportion of proliferating cells. However, many post-differentiated NSCs migrated and proliferated during neuronal differentiation until day 12. At day 12, post-differentiated NSCs proliferated everywhere. There is also strong migration of d20 neurons but less proliferation until day 12. However, at day 12, these neurons proliferated almost exclusively at the position of the printed droplets.

3.5. Maintenance of multipotency

The maintenance of multipotency of printed NSCs is demonstrated in the panels of **Figure S2** (in Supplementary File). Stem cell marker nestin (green), PAX6 (red), SOX2 (red) and β3-tubulin (green) are depicted together with Hoechst 33342 cell nuclei staining (blue) and phase contrast imaging at day 2 post-printing with different microscope magnifications. Obviously, all cells still expressed these stem cell markers at day 2.

3.6. Neuronal differentiation of NSCs and neurons after printing

The composition of cell types and the ratio of neurons to NSCs changes during culture under neuronal differentiation conditions. Figure 3D shows early-born cortical neuron nuclei marker TBR1 staining (red) and MAP2 staining (red) together with Hoechst 33342 cell nuclei staining (blue) of printed NSCs and d5 neurons, respectively, 22 days after printing (day 22 pp, diff 0/20 for NSCs; day 22 pp, diff 5/22 for d5 neurons). In the TBR1 images, the position of four printed droplets can still be seen due to the blue Hoechst staining, while there is only one droplet position depicted in MAP2 images due to higher resolution microscopy. It can be seen that printed NSCs, which were under differentiation culture conditions, migrated and populated the whole depicted region, although the highest cell density remained at the droplet positions. Most of the NSCs, post-differentiated for 20 days, were TBR1-positive and about half of them were MAP2-positive, indicating an abundant presence of early-born cortical neurons. D5 neurons showed less migration and proliferation. They were much more concentrated in the printed positions and arranged in ring-like formations. Less than 50% of d5 neurons were TBR1-positive 22 days after printing, but the proportion was higher among migrated cells and lower in the printed positions. This difference did not exist in MAP2 expression, which is generally much higher.

Further culturing under neuronal differentiation conditions led to specific differentiation in different neuronal lineages; glutamatergic and GABAergic neurons are the most common ones among these lineages. Figure 3G shows vGLUT1 staining (green) for glutamatergic neurons and GABA-antibody staining (red) for GABAergic neurons of printed NSCs (same sample and image section for both staining) at day 30 post-differentiation (d32 pp, diff 0/30). The comparison of the panels indicates that most of the NSCs differentiated to glutamatergic neurons and a smaller proportion became GABAergic neurons, which is a common proportion in the cerebral cortex; ratios of approximately 70%–80% glutamatergic and 20%–30% GABAergic neurons have been reported by other groups[60,61].

3.7. Differentiation of NSCs to glial cells under neuronal differentiation conditions

Besides differentiation to neurons, NSCs are also capable to differentiate to glial cells, such as astrocytes and oligodendrocytes. Such differentiation also occurs spontaneously, even under culture conditions supporting neuronal differentiation. Hence, differentiation of printed NSCs to astrocytes (Figure 3E) and oligodendrocytes (Figure 3F) under neuronal differentiation conditions was investigated.

The differentiation to astrocytes in neuronal differentiation medium is shown in Figure 3E with the markers GFAP (red), MAP2 (green), S100B (green, for mature astrocytes), and Hoechst 33342 (blue) at day 2 (day 2 pp, diff 0/0), day 23 (day 23 pp, diff 0/21), and day 37 (day 37 pp, diff 0/35) post-printing. These staining reveal that there are no GFAP-positive astrocytes at day 2 before starting neuronal differentiation. In contrast, there are already many GFAP-positive astrocytes at day 23. However, these cells did not increasingly appear at the position of the printed droplets but often in the interspace and mixed with neurons (MAP2-positive). At day 37, most astrocytes are mature (S100B-positive).

Figure 3F shows staining with oligodendrocyte marker O4 and Hoechst 33342 at day 2 (day 2 pp, diff 0/0), day 35 (day 35 pp, diff 0/33), and day 67 (day 67 pp, diff 0/65) post-printing. While we observed no O4-positive cells at day 2 before starting neuronal differentiation, there was already an abundance of O4-positive cells at day 35, most of them were pre-oligodendrocytes (with simple dendritic extensions without bifurcations) with a few immature oligodendrocytes (with a few bifurcations only). At day 67, mature oligodendrocytes (with long extensions and complex bifurcations) could also be observed.

3.8. Impact of astrocytes on NSCs and neurons under neuronal differentiation

The effect of astrocytes, added to or spontaneously differentiated from NSCs, on NSCs and d20 neurons under neuronal culture conditions for 23 days was investigated and

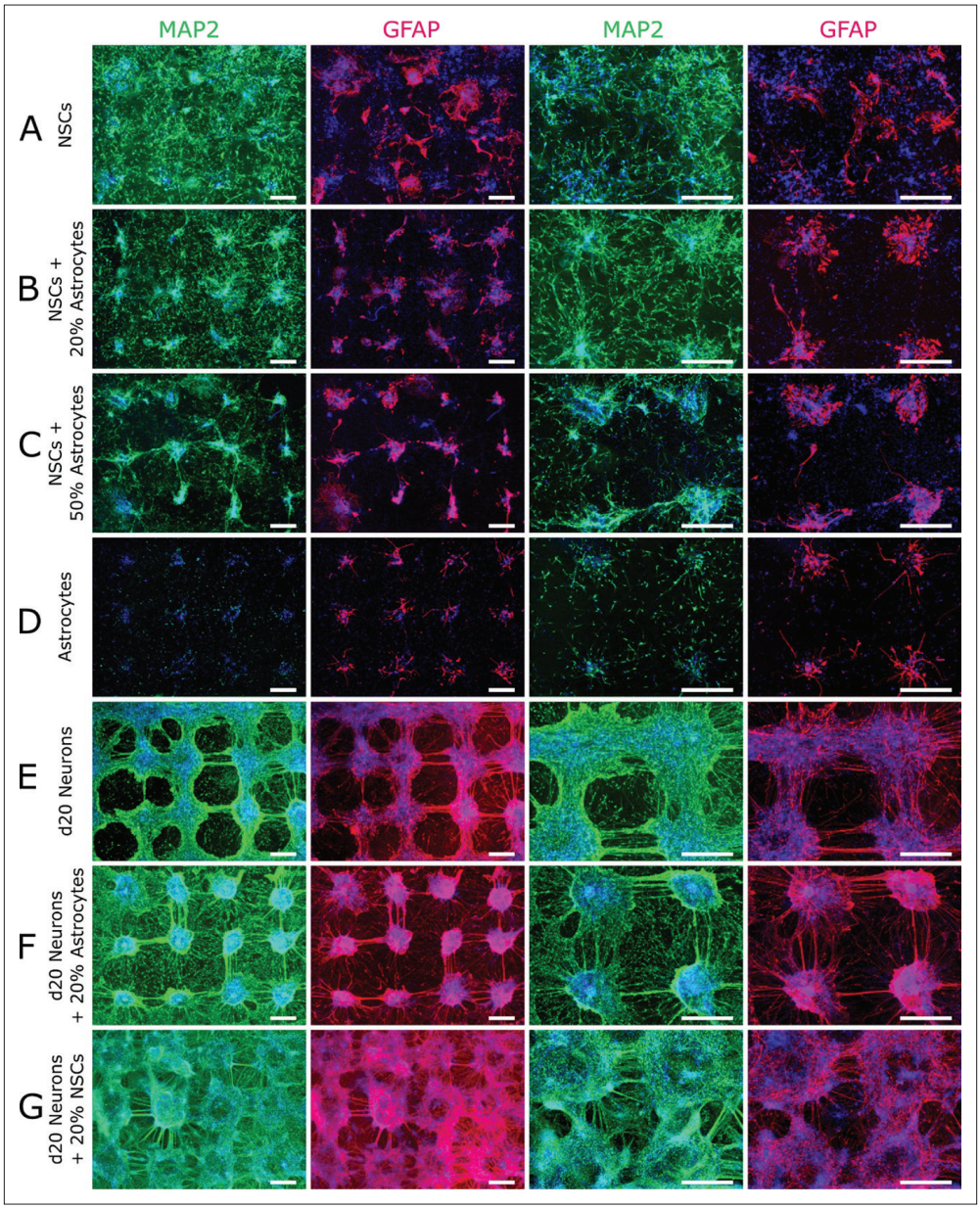

Figure 4. Printed NSCs, neurons and astrocytes 23 days post-printing. Neuronal differentiation of printed cells, compared among NSCs, NSCs with 20% of astrocytes, NSCs with 50% of astrocytes, astrocytes only, d20 neurons, d20 neurons with 20% of astrocytes, and d20 neurons with 20% of NSCs. MAP2 (green), GFAP (red), and Hoechst 33342 (blue) staining show neurons, astrocytes, and nuclei of all cells, respectively. Images with two different magnifications are depicted. Distance between droplets in printed patterns is 1 mm; scale bar: 500 μm.

results are depicted in Figure 4. For comparison, astrocytes from astrocytic differentiation of NSCs were also printed and cultured for 23 days under neuronal culture conditions (Figure 4D). MAP2 was stained for neurons (green) and GFAP for astrocytes (red), while Hoechst 33342 was used for general cell nuclei staining (blue). Due to spontaneous differentiation, there were approximately 0.1% astrocytes within NSCs at passage 5 and approximately 0.4% within d20 neurons prepared for printing (Figure 1C).

We observed strong proliferation and migration when printing NSCs only (Figure 4A), thus the printed patterns were barely recognizable after 23 days. In contrast, astrocytes did not proliferate and migrate considerably (Figure 4D). When NSCs were printed together with astrocytes, NSCs' migration was significantly reduced with 20% astrocytes (Figure 4B) and even more with 50% astrocytes (Figure 4C). The clear visibility of the printing pattern proves the lack of migration.

There was only slight migration of d20 neurons (Figure 4E) compared to NSCs (Figure 4A); however, d20 neurons (which also contained NSCs and a few spontaneously differentiated astrocytes) still proliferated. Several connections between printed droplets developed. Nevertheless, the printed pattern was clearly visible 23 days after printing. When 20% astrocytes were added to neurons before printing, the pattern (Figure 4F) was compact 23 days after printing compared to neurons alone (Figure 4E), although there were more MAP2-positive neurons in the space between these droplets. Similar to neurons alone, several connections had formed between printed droplets. Furthermore, addition of 20% of NSCs to neurons before printing was investigated. In this case, much more cells were observed after 23 days (Figure 4G), with higher proliferation and migration. There were also several connections between the printed droplets; however, the space between these droplets was filled with so many migrated cells that the printing pattern was barely visible in some places.

Remarkably, the percentage of astrocytes 23 days after printing does not seem to considerably depend on the percentage of astrocytes at the time of printing, except, of course, for the case of printing of astrocytes alone (Figure 4D). Furthermore, the percentage of astrocytes in NSCs cultured for 23 days under neuronal differentiation condition post-printing was much higher than the percentage of astrocytes in d20 neurons (pre-differentiated in 2D culture) at the day of printing (≈ 0.4%).

3.9. Formation of synapses during differentiation of printed NSCs and neurons

Neurons develop their full functionality with the establishment of spontaneously active neuronal networks. For communication within these networks, the formation of synapses (synaptogenesis) is crucial. Synapses consist of pre- and post-synaptic compartments of two connecting neurons, at which neurotransmitters are transmitted from the pre-synaptic cell to the post-synaptic one. The pre- and post-synaptic compartments consist of different proteins and are positioned with a small gap (synaptic cleft) in between. These compartments can be observed in juxtaposition or as colocalization (overlapping).

In Figure 5, synaptic compartments of printed NSCs (Figure 5A and 5B) and d20 neurons (Figure 5C and 5D), neuronal post-differentiated for 20 days (day 22 pp, diff 0/20 for NSCs; day 20 pp, diff 20/20 for neurons), are depicted by pre-synaptic synaptophysin staining (red) and post-synaptic PSD95 staining (green) together with Hoechst 33342 cell nuclei staining (blue). The yellow color in the right column panels is an overlap of red and green staining. Both synaptic markers were found in abundance after 20 days of neuronal pre-differentiation in both NSCs as well as d20 neurons, and synaptic compartments can be seen on the right panels of (B) and (D) in juxtaposition and in colocalization. This abundance demonstrated neuronal maturation, extensive formation of synapses, and connection of neurons via synapses to form neuronal networks.

3.10. Dependence of neuronal activity on printed cell type

Collective neuronal activity always involves an increase of the level of calcium ions (Ca^{2+}). The intracellular calcium concentration of neurons at rest is about 50–100 nM, but transiently rises to ten- or hundred-times higher levels during electrical activity[62,63]. Therefore, electrical activity of neuronal circuits was monitored by imaging of calcium levels using the calcium-binding fluorochrome Fluo-8 AM in combination with a wide-field fluorescence microscope with video camera.

The neuronal activity of cells depended on cell type and duration of pre-differentiation. However, there were strong variations in activity between samples handled equally with the same printing parameters and biomaterials. The cells' activity was visualized by calcium imaging and roughly rated by applying a grading system ranging from 0 (no activity) to 24 (abundant and intensive activity with bursting events). Figure 6A depicts the mean of these ratings for different cell types (NSCs, d20 neurons, astrocytes, and mixtures of these). Data were averaged over different durations of post-differentiation. Figure 6B lists the statistical *P* values, which are highlighted in red whenever they are below the significance level of 0.05.

Noticeably, NSCs show higher levels of activity than pre-differentiated neurons. The activity of mixtures of NSCs with 20% (activity 8.6 ± 0.5) or 50% (9.3 ± 1.0) astrocytes was similar to the activity of NSCs only (8.9 ± 0.3; no significance), while the activity of mixtures of neurons with 20% astrocytes (6.2 ± 0.6) or 20% NSCs (6.4 ± 0.8) was lower than that of neurons only (7.7 ± 0.5; no significance). The activities of these neuron-based mixtures were also significantly lower than those of NSCs or NSC-based mixtures, while there was no significant difference between neurons only and NSCs. Additionally, the activity of astrocytes only (4.2 ± 0.9), which is the lowest, is depicted for comparison.

3.11. Development of neuronal activity in long-term cultivation

Samples of NSCs printed with bioink on Matrigel™ started to show spontaneous activity at day 10 of differentiation (day 12 pp, diff 0/10; **Videoclip S1**). Activity became widespread from day 25 onward (day 27 pp, diff 0/25;

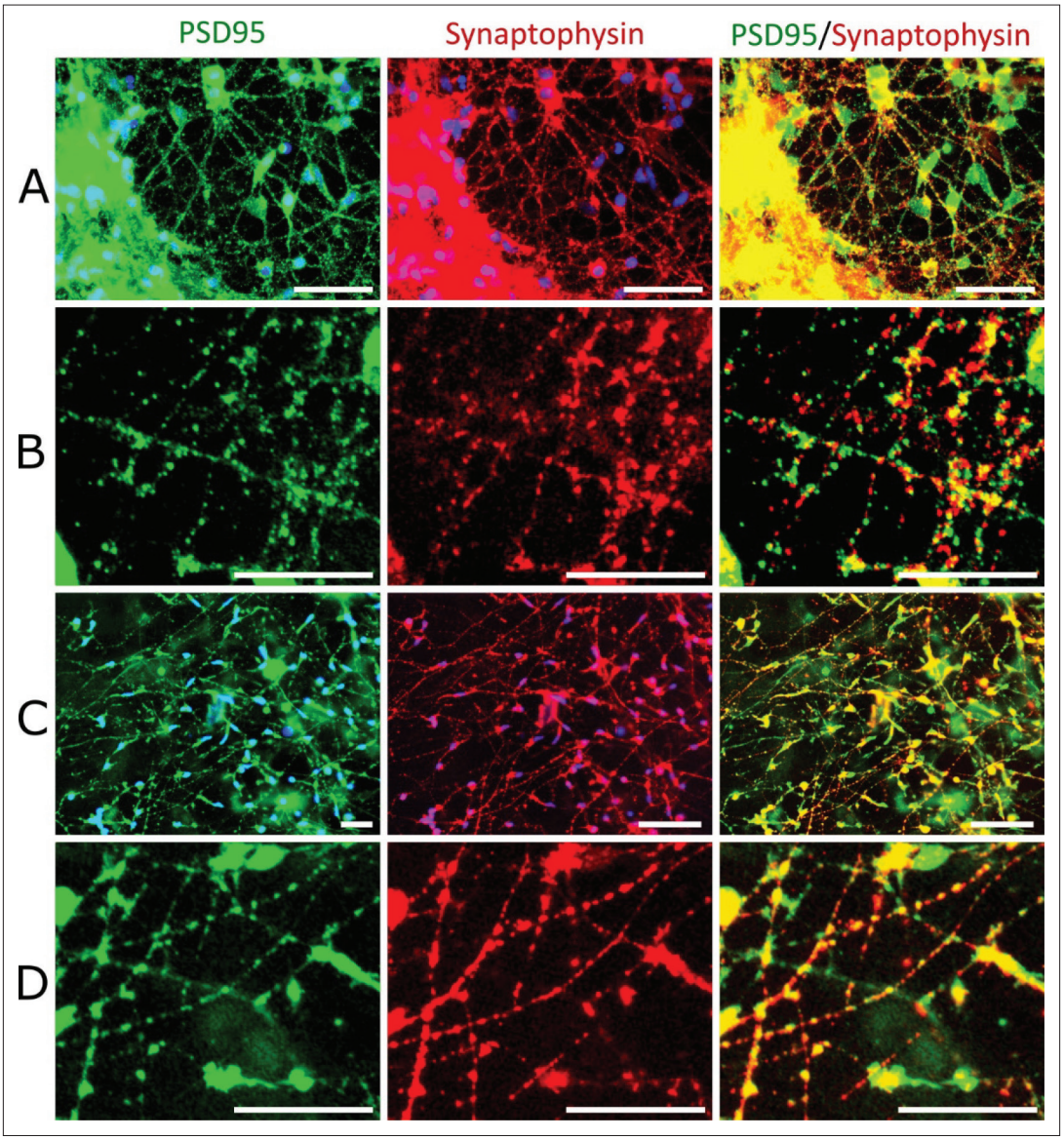

Figure 5. Formation of neuronal networks and synapses. Development of pre- and post-synaptic compartments by printed NSCs (A and B) and d20 neurons (C and D), both neuronal post-differentiated for 20 days and stained with pre-synaptic synaptophysin (red) and post-synaptic density protein PSD95 (green) together with Hoechst 33342 cell nuclei staining (blue). (B and D) Details of (A) and (C), respectively. For each panel (A–D), the right image is a merger of the others; the yellow color in these merged images is an overlap of red and green color. Both synaptic markers were found in abundance after 20 days of neuronal differentiation, and synaptic compartments could be seen in juxtaposition (red and green spot next to each other) and in colocalization (yellow spot as overlap of red and green spot). This demonstrates neuronal maturation, extensive formation of synapses, and connection of neurons via synapses. Scale bar: 50 μm.

Videoclip S2), with bursting events emerging by day 37 of differentiation (day 39 pp, diff 0/37; Videoclip S3). Further cultivation under differentiation conditions up to day 65 of differentiation did not increase the average observed activity. It must be noted, however, that there was always large variation across samples, with ones depicting low activity and others exhibiting abundant and intense activity.

The spontaneous activity of neurons printed with hyaluronic acid on Matrigel™ did also increase with the duration of pre-differentiation (data not shown). However, the average observed activity was always a bit lower than that of NSCs and the number of average bursting events directly visible was considerably lower. An illustrative recording at day 26 (day 26 pp, diff20/26) is shown in Videoclip S4.

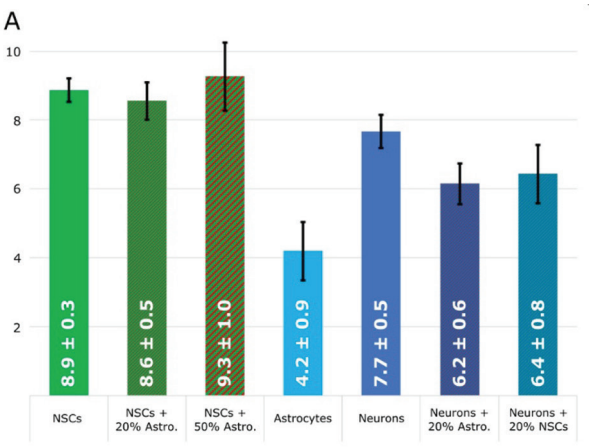

B p-values

	Neurons + 20% NSCs	Neurons + 20% Astro.	Neurons	Astrocytes	NSCs + 50% Astro.	NSCs + 20% Astro.
NSCs	0.0225	0.0083	0.0875	0.0006	0.7685	0.6781
NSCs + 20% Astro.	0.0330	0.0071	0.2271	0.0002	0.5354	
NSCs + 50% Astro.	0.0412	0.0061	0.1466	0.0006		
Astrocytes	0.0879	0.0588	0.0016			
Neurons	0.1866	0.0708				
Neurons + 20% Astro.	0.7805					

Figure 6. Functionality of neuronal network dependence on cell type. (A) Rating of the neuronal activity visualized by calcium imaging applying a grading system ranging from 0 (no activity) to 24 (abundant and intensive activity with bursting events). Different printed cell types and cell compositions were differentiated post-printing with different durations of neuronal differentiation period. Mean and standard error of mean (SEM) of the ratings for the activity of NSCs (8.9 ± 0.3), NSCs mixed with 20% (8.6 ± 0.5) or 50% (9.3 ± 1.0) of astrocytes, astrocytes (4.2 ± 0.9) alone, d20 neurons (7.7 ± 0.5), and d20 neurons mixed with 20% of astrocytes (6.2 ± 0.6) or NSCs (6.4 ± 0.8) are depicted, and also averaged over different durations of neuronal post-differentiation period. (B) Statistical analysis of *P* values for unpaired two-sample *t*-test, which are highlighted in red if less than the significance level of 0.05.

3.12. Formation of neuronal networks and co-activation/bursting events

A measure for formation of functional neuronal networks is the appearance of collective activation events, which were quantified by computer-based analysis of calcium imaging videos. The procedure of this analysis is shown in Figure 7. The images from a given experiment were analyzed to identify neurons (Figure 7A) and extract their fluorescence traces (Figure 7B). Sharp peaks in fluorescence revealed activity, and several neurons co-activating synchronously in the same time window (yellow box) evinced the bursting events. As shown in Figure 7C, fluorescence traces were analyzed to extract the timing of neuronal activity, generate the raster plots and inspect the data for strong episodes of collective activity (blue dots). Data were then further analyzed to identify communication among neurons and characterize the functional organization of the neuronal circuits (Figure 7D and 7E), as discussed later.

The development of the network after printing under neuronal differentiation conditions is shown in Figure 8A and 8B. Panels depict the raster plots of activity for 1,000 individual neurons on top, and the averaged activity (termed "global network activity") at the bottom. Figure 8A shows the development of printed neurons 27 (left), 39 (middle) and 67 (right) days in differentiation medium after printing. For comparison, Figure 8B shows the development for cells that were neuronally pre-differentiated for 5 days, printed, and then cultured in differentiation medium for additional 22 (left), 44 (middle), and 67 (right) days after printing. We note that, for printed NSCs, no collective activity could be observed at 27 days in the example shown. However, the time of the first appearance of bursting events varied among experimental realizations, and thus in other experiments with NSCs of different passages we already observed bursting events before day 20. Overall, the panels reveal a gradual increase of activity, with clear bursts at day 39 that become stronger at day 67 and later. Thus, there is a clear evolution of burst over time. In the case of pre-differentiated neurons, these collective activity events could already be observed after 22 days (or 27 days of total differentiation time) and even earlier, i.e., significantly earlier than with printed NSCs. However, there was no further development over time. Indeed, by day 67, the bursting events remained weak, comparable in number and strength as those observed at day 22. To better contrast the differences between the two culture conditions, extended over all culture realizations, Figure 8C shows a statistical analysis of the development of mean neuronal activity over time, while Figure 8D compares the strength of the collective activity (bursting events) of printed NSCs and pre-differentiated neurons. The gradual increase of network activity for NSCs over time is clear, and contrasts with the weak and practically constant activity of pre-differentiated printed neurons. The distribution of burst sizes is also remarkably different. While burst sizes practically double for NSCs along development (from 11% of the network to 27%), they remain small (by 5%–10% of the network) for pre-differentiated neurons.

3.13. The effect of added astrocytes

One aspect of this study is the effect of added astrocytes on neuronal network formation. It must be considered that NSCs can spontaneously differentiate into astrocytes even under neuronal differentiation conditions. This means that even without the addition of astrocytes, they can already be contained in the cultures. However, we observed only a proportion of approximately 0.1% astrocytes in NSCs at passage 5 and approximately 0.4% astrocytes in d20 neurons.

Figure 9 shows the effect of added astrocytes on the fraction of printed NSCs that were organized as neuronal

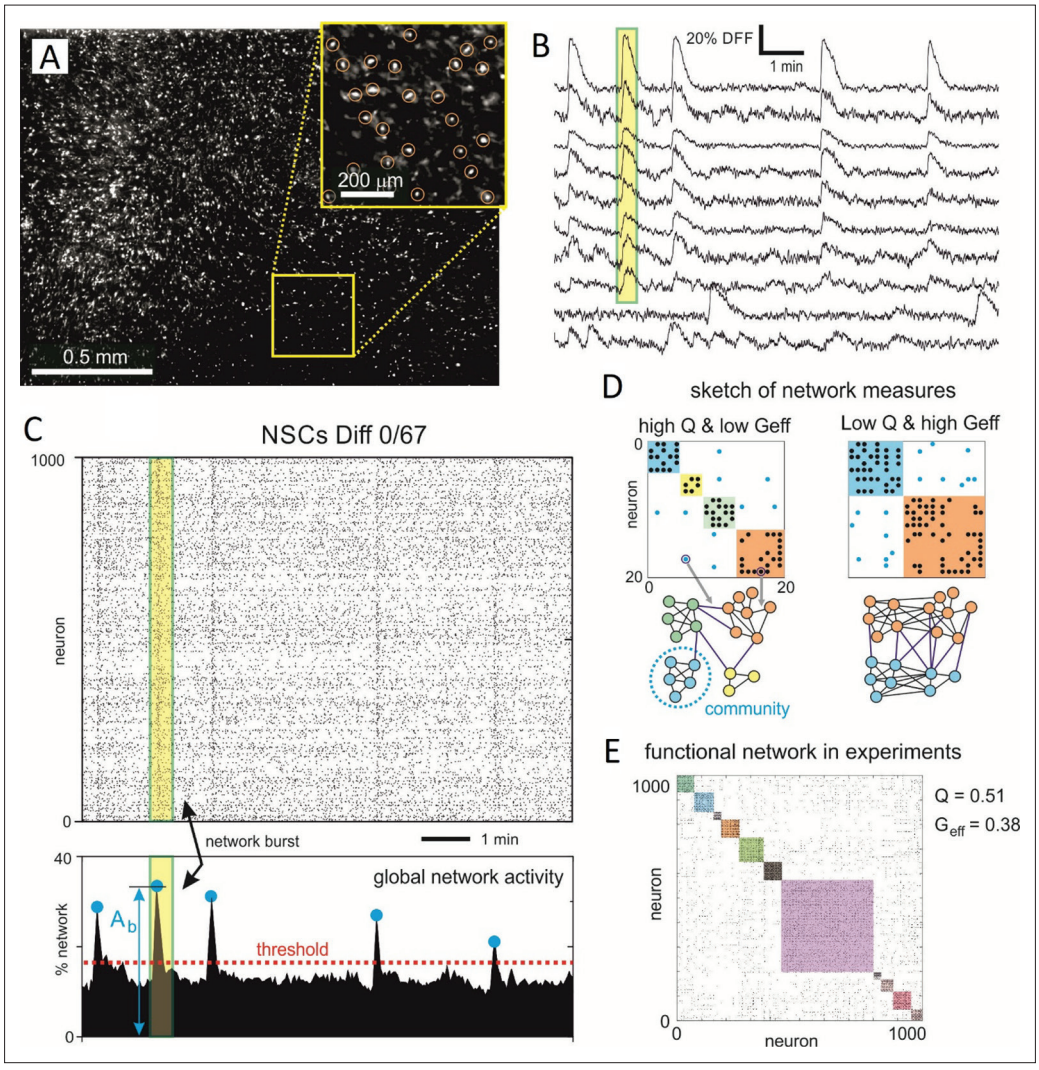

Figure 7. Data acquisition and analysis. (A) Highly contrasted fluorescence image of NSCs at Diff 0/67. Bright spots are neural cells (neurons and glia). The enlarged area shows detail of the field of view, with the brightest spots (yellow outlines) automatically ascribed as regions of interest (ROIs). (B) Fluorescence traces of spontaneous activity for 10 randomly selected ROIs. Sharp increases in fluorescence reveal neuronal activity and are associated to elicited action potentials. The simultaneous activation of a group of neurons shapes a network burst (yellow rectangle). (C) Top: Raster plot of spontaneous activity extended to 1000 neurons. Black dots are neuronal activations. Network bursts appear as vertical bands of coordinated activity. Bottom: Corresponding "global network activity" revealing a persistent background activity of about 10% of the network and 5 significantly strong peaks that correspond to network bursts (blue dots and yellow rectangle). (D) Sketch of functional connectivity and network measures for two contrasting situations of a highly segregated network (left) and a highly integrated one (right). The top matrices show the functional communities as colored boxes along the diagonal. Dots are functional connections, either intra-modular (black) or inter-modular (blue). The bottom graphs show the corresponding network maps. (E) Functional connectivity matrix of the experiment shown in panels A–C, highlighting the functional communities. The combination of moderate Q and low G_{eff} values indicates a network that exhibits clear functional communities that are well linked among themselves, suggesting a balanced network.

networks after 25 days under neuronal culture conditions. Zero, 20, or 50% added astrocytes indicate that, prior to printing, for every 100 NSCs, a number of 0, 20, or 50 astrocytes were added, respectively. There were only small bursts observed without added astrocytes (on average, 7 ± 4% of the networks' cells were involved in one burst) or with 20% of added astrocytes (6 ± 2%), but significantly larger bursts (14 ± 4%) when 50% of astrocytes were added.

A detailed representation of the impact of astrocytes on neuronal network connectivity is shown in Figure 10A. The functional organization of printed NSCs after 25 days under neuronal differentiation culture conditions without added astrocytes is depicted on the top row. The left panel shows the functional connectivity matrix, i.e., the neurons that frequently exchanged information. Each color of the eight boxes along the diagonal represents one functional neuronal community, understood as a group of neurons that tend to

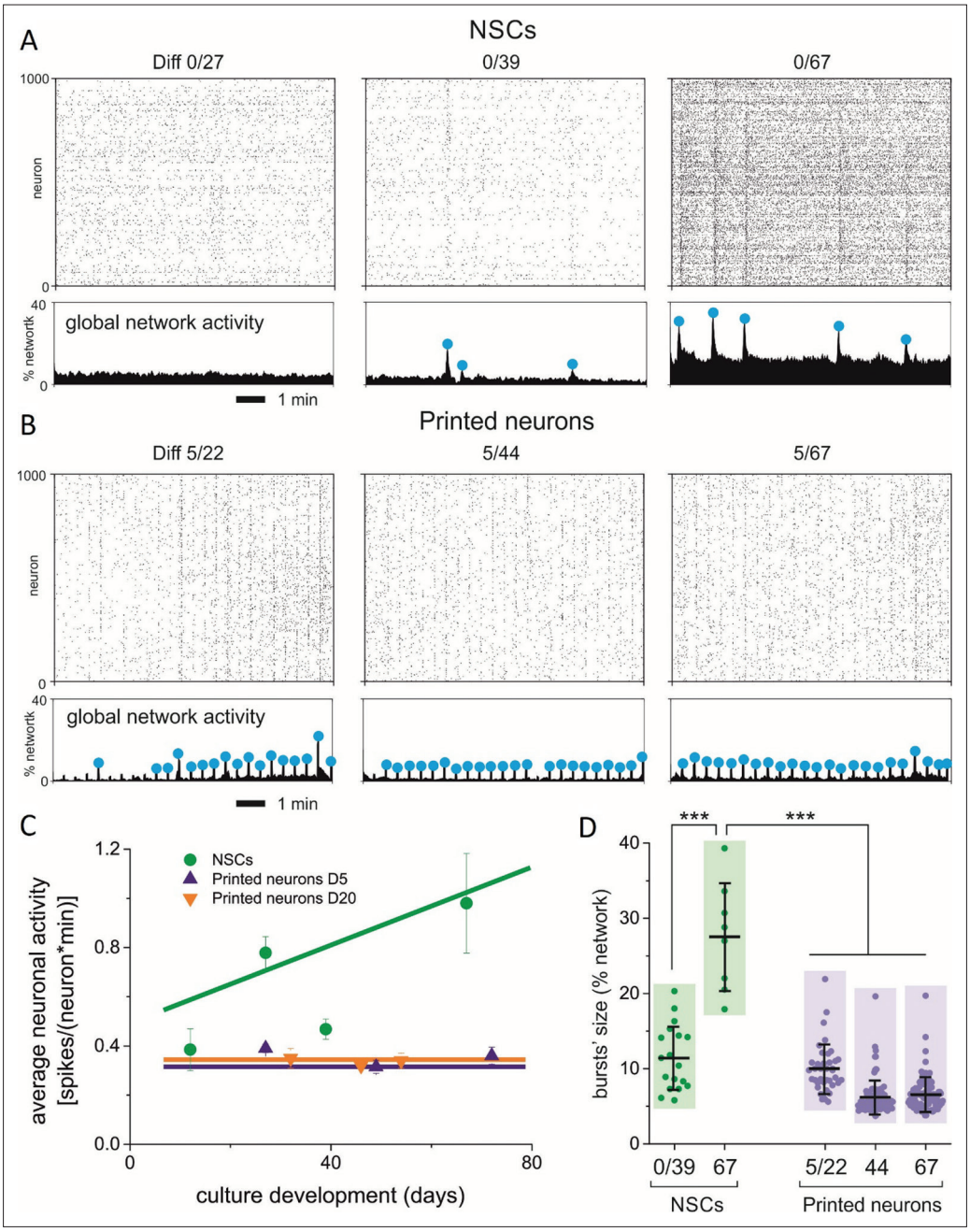

Figure 8. Contrasting activity between NSCs and printed neurons. (A) Representative raster plots (top) and global network activity (bottom) of NSC cultures along development, showing the emergence of collective activity in the form of network bursts and the progressive increase of burst sizes (blue dots). (B) Corresponding data plot for printed neurons. Bursts emerge since early days in culture but remain small. Spontaneous activity is overall weaker than NSCs at late developmental times. (C) Comparison of average neuronal activity for NSCs and printed neurons along development. Activity in NSCs gradually increases along time, while printed neurons maintain a low activity. Data are shown as mean ± standard error of mean. Each data point is an average over four cultures, and lines are linear fits. (D) Comparison of burst sizes between NSCs and d5-printed neurons. Burst sizes for NSCs significantly increase along development and are much higher than for printed neurons. Color boxes show the extent of the distribution; dots are all the burst sizes observed in four realizations of each condition, and black crosses indicate mean ± standard deviation. Significance analyzed by a multiple comparison test in ANOVA. *** $P < 0.001$.

communicate within the group more strongly than with the rest of the network. The central panel shows the networks as a map with colored dots indicating neurons integrated in the respective network. A larger dot size indicates higher connectivity. The eight identified neuronal communities are not spatially separated, but all extend over the full observation area (2×1.5 mm^2) and overlap each other. This finding indicates the existence of neuronal connections at

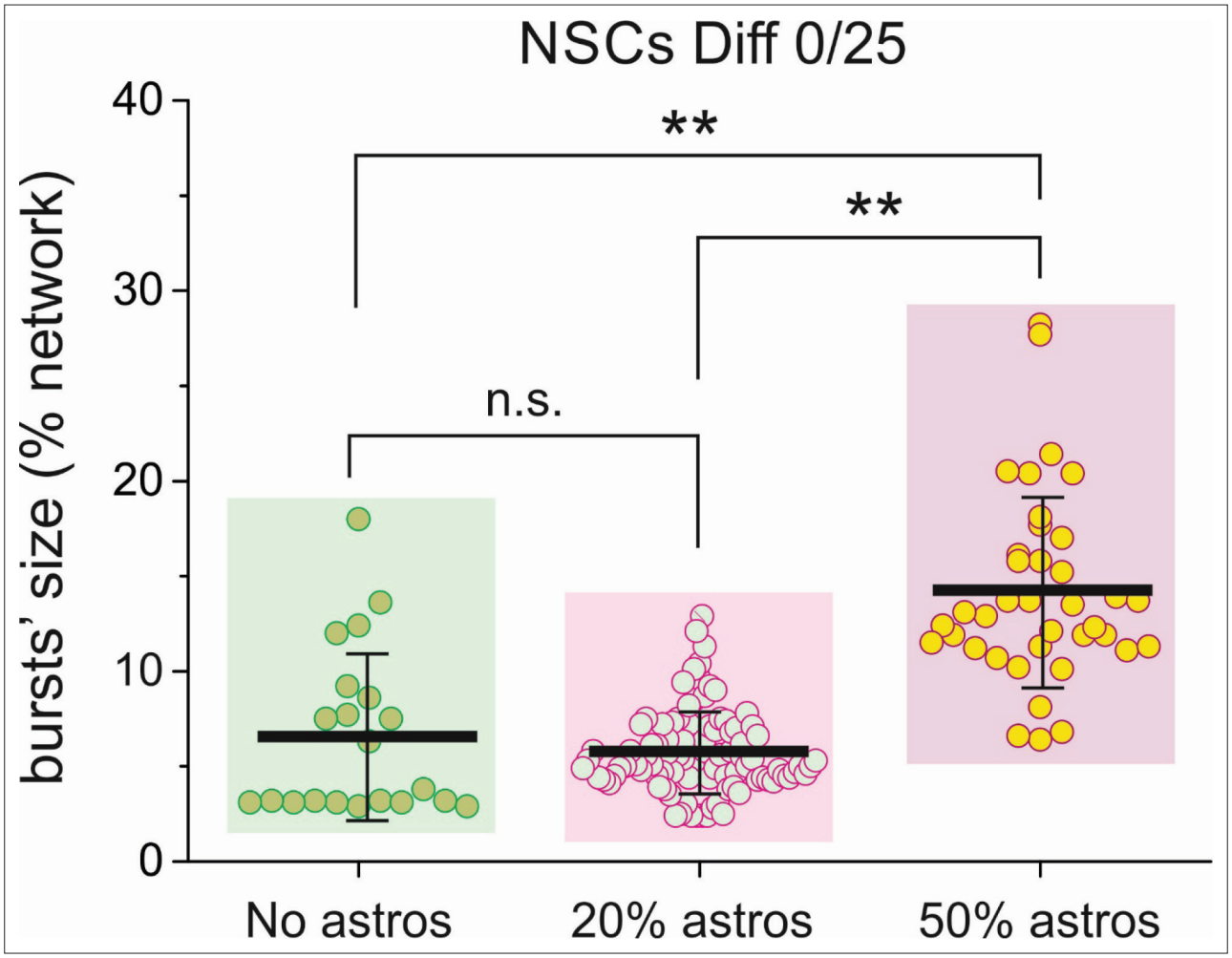

Figure 9. Impact of astrocytes on network bursts. Comparison of burst sizes in NSC cultures at Diff 0/25 with and without astrocytes. Cultures with 20% astrocytes behave similarly as those without astrocytes, with average burst sizes of about 7% of the network. Cultures with 50% astrocytes exhibit a significant increase in burst size, of about 15% of the network on average, and indicate an excessive synchronization of the neurons. Significance analyzed by a multiple comparison test in ANOVA. ** P<0.01.

both short and long distances. An alternative topological representation of the functional neuronal communities is depicted in the right panel, in which neurons are grouped by community, and communities are separated according to their coupling within the network. A similar representation of printed NSCs with 50% astrocytes under same culture conditions is shown at the bottom row of Figure 10A. Here, too, all networks are extended over the entire observation section. However, there are less communities (five instead of eight), which are clearly much larger. The overall higher cohesion of the network is also shown in the topological representation, where communities are closer to one another. Altogether, the results indicate that astrocytes accentuate the synchronization among neurons and therefore strengthen their functional interactions, shaping a network where neurons are strongly coupled. Without the addition of astrocytes, a network where neurons are relatively more isolated was shaped. We must note that both culture types are active and healthy. The increased network functional cohesion when astrocytes are present is not necessarily advantageous since neuronal circuits must balance local and global communication for optimal functioning, but indicates that the presence of astrocytes is central in shaping global network activity.

To statistically analyze the differences in network functionality with and without astrocytes, we compared two network measures, namely global efficiency G_{eff} (left) and community statistic Q (right), for culture realizations without, with 20% and with 50% astrocytes, as shown in Figure 10B. The global efficiency captures the degree of overall network communication (see also Figure 7D) and is significantly higher for cultures with 50% astrocytes, which indicates an increased cohesion of the functional networks and that is

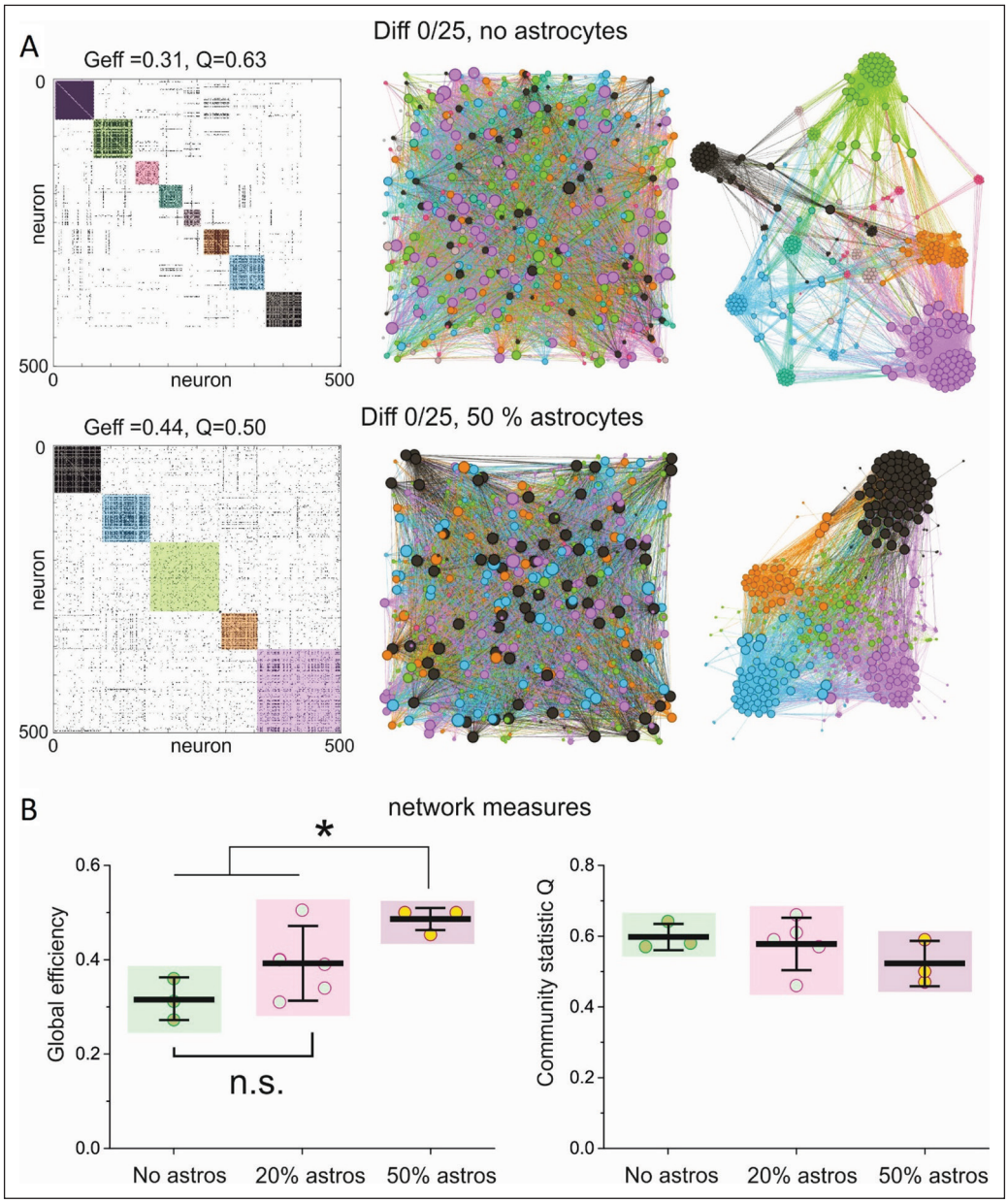

Figure 10. Impact of astrocytes on functional connectivity. (A) Example of the functional organization of an NSC culture. The left panel shows the adjacency matrix with boxes along the diagonal that correspond to functional communities. The central panel shows the corresponding network map, with neurons indicated as dots and color-coded identically as in the matrix. The larger the diameter of a dot, the higher its connectivity. Neurons belonging to a given community extend all over the culture, indicating that neurons connect both at short and long length scales. The right panel provides an alternative topological representation of the functional communities, in which neurons are grouped by community, and communities separated according to their coupling within the network. Orange and black communities are relatively isolated, while the pink one is strongly coupled. (B) Comparison of two network measures, global efficiency G_{eff} (left) and community statistic Q (right), for cultures with and without astrocytes. G_{eff} is significantly higher for cultures with 50% astrocytes, indicating an excessive cohesion of the functional network and that is a consequence of the elevated bursting observed in these cultures. Q gradually decays with the number of astrocytes, indicating a progressive strengthening of network integration. Significance analyzed by a multiple comparison test in ANOVA. *$P < 0.05$.

a consequence of the elevated bursting observed in these cultures (Figure 9). The community statistic Q, which captures the number and isolation of communities in the networks, gradually decreased with the percentage of added astrocytes, indicating that astrocytes increased network integration.

4. Discussion

The main objectives of this study were the investigation of 3D laser-based bioprinting of neural constructs and to delineate whether NSCs are preferable over

pre-differentiated neurons. In the latter case, it is also important to ascertain which stage of differentiation is optimal. Essential aspects were viability, maintenance of stemness and differentiation potential, as well as ability to form functional neuronal networks.

An aspect for future research will be the identification of other biomaterials for printing, bioinks and culture substrates, which probably could even better support formation of functional neuronal networks; however, we applied Matrigel™ as substrate, and hyaluronic acid and cell culture media as bioink in the present study, since one of our previous studies found that these materials are the best for printing hiPSCs[45], from which all cells applied in the present study were generated.

These generated cell types were not present as homogeneous cultures. NSCs at passage 3–5 that were printed already contained some TBR1- and MAP2-positive cortical neurons due to spontaneous differentiation, and a few cells (≈ 0.1%) differentiated toward astrocytes at passage 5. However, no astrocytes were observed in NSCs at passage 3, and no oligodendrocytes were observed at any of these passages. On the other hand, d20 neurons still contained undifferentiated NSCs and some astrocytes (≈ 0.4%), but over 80% of cells were MAP2-positive. We found that there were more than 90% GFAP-positive cells within astrocytes. Furthermore, it can be noted that very few astrocytes were generated under neuronal differentiation and very few neurons developed under astrocytic differentiation conditions in conventional 2D cell culture; in contrast, many more astrocytes were generated under neuronal post-differentiation in printed 3D cell samples. Especially for long-term cultivation post-printing, the compositions of different cell types need to be taken into consideration.

Initially, the viability post-printing was studied, which is affected not only by the printing process itself and the applied biomaterials; harvesting neurons from culture plates caused dissociation of neuronal networks that were spontaneously formed in cell culture and can reduce viability. Figure 2C demonstrates this effect. Even control neurons that were not printed and were not in contact with any of the biomaterials, bioink, or culture substrate showed a reduced viability that decreased with the duration of pre-differentiation to 68.4 ± 0.8% for d20 neurons. We assume that neurons were harmed due to chemical and mechanical dissociation by pipetting required to dissolve networks formed under differentiation culture conditions (depicted in **Figure S1**). On the other hand, the printing process and the applied biomaterials, hyaluronic acid and Matrigel™, did not reduce viability. On the contrary, the viability of printed cells was higher, significantly in five out of eight cases, than the viability of donor and control cells. We hypothesize that cell viability is cell density-dependent, and that the higher viability of printed cells is caused by the high density of cells concentrated in printed droplets compared to the density of donor and control cells seeded homogeneously by pipetting with the same total amount of cells per area. In contrast to neurons, the viability of NSCs is much higher and about 91.1 ± 0.5% for control cells and 94.5 ± 0.6% for printed cells, which is in good accordance to 92 ± 3% reported by Sharma et al.[32] for printing of hiPSC-derived NSCs, while other groups reported lower viability of 75%–80%[28,35] for printing of NSCs. Salaris et al.[30] reported viability of 78 ± 4% for hiPSC-derived neurons. However, in these studies a different extrusion-based bioprinting technique was applied; therefore, the results were not directly comparable. By applying a similar laser-based bioprinting technique and rat dorsal root ganglion neurons, Curley et al.[23] demonstrated a viability of 84.9 ± 4.7% for printed cells, 86.4 ± 3.3% for donor cells, and 89.3 ± 2.0% for control cells. Compared with these results, we achieved higher viability for NSCs and d5 neurons, but lower viability for d10 and d20 neurons. Furthermore, Curley et al.[23] did not observe higher but lower viability for printed cells.

In our study on printing of hiPSCs with the same biomaterials, we achieved generally lower viability of printed (82 ± 1%), donor (84 ± 1%), and control cells (87 ± 1%); here the viability of printed cells was significantly lower than the control cell viability. However, pluripotent hiPSCs are known to be sensitive to environmental parameters, such as culture media components, paracrine factors, and matrices. These factors have an impact on cell viability and proliferation; when dissociated into single cells, programmed cell death (apoptosis) of hiPSCs is immediately induced. The present study confirmed that, in comparison to hiPSCs, hiPSC-derived multipotent NSCs are less delicate.

Obviously, NSCs proliferate much more than pre-differentiated neurons. Figure 3C suggests that proliferation of neurons, in opposite to NSCs, depends on cell density, which is in line with the fact discussed above that neurons, like NSCs, concentrated in printed droplets showed higher viability than cells homogeneously seeded by pipetting.

Printed NSCs maintained their multipotency, if cultivated under expansion culture conditions, as demonstrated by stem cell markers nestin, SOX2, and PAX6 (**Figure S2B** and **2C**). On the other hand, if NSCs were cultivated under neuronal differentiation conditions after printing for 20 days, many TBR1- and MAP2-positive cortical neurons could be observed (Figure 3D), while among printed d5 neurons cultivated for further 22 days

under neuronal differentiation conditions, only a few were TBR1-positive but most of them were MAP2-positive (Figure 3F). Printed neurons lost the early-born cortical neuron marker TBR1 during further differentiation.

Under neuronal differentiation conditions for 30 days, printed NSCs already express glutamatergic and GABAminergic neuron lineage markers vGLUT1 and GABA; thus, within this period, printed NSCs undergo all differentiation stages from stem cell to specific neuronal lineage. Aside from that, spontaneous differentiation toward glial cells also occurred under neuronal differentiation conditions, and even mature oligodendrocytes (Figure 3F) and astrocytes (Figure 3E) were observed. Similar findings were also reported by other groups[29,30,34,35].

As shown in Figure 4, the spontaneous differentiation to astrocytes under neuronal differentiation conditions was much higher for printed NSCs and d20 neurons than for normal cell culture (≈ 0.1% for passage-5 NSCs, ≈ 0.4% for d20 neurons; Figure 1C). Also noticeable was the proportion of astrocytes after prolonged cultivation under neuronal culture conditions of printed samples with and without added astrocytes (Figure 4); this does not seem to have been dependent on the proportion of astrocytes at the time of printing. We assume that both might be due to the high cell concentration in the 3D-printed droplets compared to 2D cell culture[34,35].

Figure 5 demonstrates synaptogenesis and formation of neuronal networks by printed NSCs and d20 neurons cultivated under neuronal differentiation conditions for 20 days post-printing. We did not observe difference in synaptogenesis between NSCs and d20 neurons; however, the formation of dendrites and thus the neuronal networks during differentiation of printed NSCs depended on cell density. Better results were achieved in bigger droplets with more cells (Figure 2D and 2E). Formation of synapses by printed hiPSCs, differentiated 30–37 days post-printing, was also reported by Gu et al.[34,35].

An important part of the experiments within this study was the calcium imaging analysis of printed NSCs, pre-differentiated neurons, astrocytes and compositions of this cell. Calcium imaging demonstrates functionality of neuronal networks by visualizing spontaneous activity and collective activity of several neurons (bursting events).

Our study revealed that there was no clear relationship between strength of spontaneous neuronal activity and cell composition, except from the fact that the neuronal activity of astrocytes alone was strongly reduced (Figure 6). When comparing the neuronal activity of printed NSCs and pre-differentiated neurons with succeeding neuronal differentiation via calcium imaging, we found that the addition of other cell types, i.e., astrocytes to NSCs and neurons or 20% NSCs to neurons, did not lead to stronger activity and even reduced activity in the case of neurons (not significant). The observed neuronal activity of printed NSCs or NSC-based cell mixtures was always higher than the activity of printed neurons or neuron-based mixtures (significant when compared with neuron-based mixtures).

When focusing on collective neuronal activity, statistical evaluation revealed a distinct difference between NSCs and neurons, even when d5 neurons (NSCs, pre-differentiated for 5 days) were used. When NSCs were printed and cultivated under neuronal culture condition, the activity increased with time (Figure 8). Conversely, we observed collective activity earlier in neurons, even in d5 neurons; however, this collective activity did not increase any further with extended cultivation under neuronal differentiation condition. Interestingly, we did not observe considerable differences in the synaptogenesis of NSCs and d20 neurons (Figure 5); therefore, the distinct difference in collective activity was not expected.

The addition of 50% astrocytes (Figure 10) increased burst size and global efficiency of collective neuronal activity of printed NSCs significantly, while the modularity (community statistic Q) decreased; 20% astrocytes did not have a significant effect. In opposite, the spontaneous activity was not significantly affected by addition of astrocytes (Figure 6). Unexpectedly, neither the spontaneous (Figure 6) nor the collective (data not shown) activity of d20 neurons was significantly affected by added astrocytes; actually, we had expected that the astrocytes would help the neuronal network develop better[64,65]. Therefore, in terms of maximal collective neuronal activity and functionality of neuronal networks, NSCs with 50% added astrocytes were the best in our study. Moreover, the presence of astrocytes resulted in reduced migration (NSCs only) and the formation of more compact cell aggregates (NSCs and neurons) as well as supported printing pattern maintenance (NSCs and neurons).

To the best of our knowledge, this is the first study that directly compares printing of hiPSC-derived NSCs and neurons generated from these NSCs at different differentiation stages as well as investigates the impact of co-printed astrocytes. Future studies will investigate the effect of other biomaterials applied as bioink and substrate. In this study, Matrigel™, a matrix extracted from Engelbreth-Holm-Swarm mouse sarcoma, was used as a substrate only. We did not mix Matrigel™ into the bioink, but printed the bioink with cells onto the Matrigel™ substrate. For printing thick neural tissue, the effect of such a substrate is rather limited to the bottom layers. When printing thick neural tissue, results could

be different due to the spatially decreasing effect of the Matrigel™. Matrigel™ is widely used in 2D and 3D cell culture and for bioprinting as well, but its composition is rather undefined. Therefore, more defined alternatives are required for standardized test-systems. Further important aspects are the impact of different printing patterns on neuronal network formation and the interaction between different cells in these patterns, especially when printing different cells at specific positions.

5. Conclusion

NSCs could be laser-printed with high viability of about 95% and without affecting their stemness and differentiation potential. In contrast, the viability of printed neurons (pre-differentiated NSCs) decreased with duration of pre-differentiation period (below 70% for 20 days of pre-differentiation). We found significant differences in further differentiation of printed NSCs and neurons compared to normal cell culture, especially the differentiation to astrocytes under neuronal differentiation conditions was increased. This can be explained by the higher local cell density in the printed droplets—at similar average cell density. Synaptogenesis, neuronal network formation and neuronal activity of connected cells were observed during differentiation of printed NSCs and neurons. While we did not observe differences in synaptogenesis, we found distinct differences in network formation and neuronal activity.

Pre-differentiation of NSCs before printing did accelerate both neuronal network formation after printing and onset of collective neuronal activity. However, further development of frequency and intensity of collective activity was superior when NSCs were applied. Addition of astrocytes to NSCs further supported network formation and increase of collective activity, while no comparable effect was observed when astrocytes were added to neurons.

Therefore, NSCs seems to be the best choice for printing of functional neuronal networks. However, if complex systems containing neurons and other cell types shall be printed, differentiation post-printing alone might not be possible. Moreover, proliferation and migration of NSCs were stronger than those of neurons; maintenance of printed pattern was better when pre-differentiated neurons were printed. Possibly, these findings would be different if other biomaterials were applied, which better support network formation by pre-differentiated neurons. We aim to investigate this in a subsequent study.

Acknowledgments

The authors would like to thank Axol Biosciences Ltd. (Cambridge, UK) for providing NSCs and culture materials.

Funding

The research presented here was funded by European Union's Horizon 2020 projects MESO-BRAIN, Grant 713140, PLATFORMA, Grant 951890, the Ministerio de Ciencia e Innovación (Spain, Grant PID2019-108842GB-C21), the Generalitat de Catalunya (Spain, Grant 2017- SGR-1061), and German Cluster of Excellence Ex62/2 Rebirth.

Conflict of interest

The authors declare no conflicts of interests.

Author contributions

Conceptualization: Andrea Deiwick, Lothar Koch
Formal analysis: Lothar Koch, Jordi Soriano
Funding acquisition: Boris Chichkov, Jordi Soriano
Investigation: Andrea Deiwick, Lothar Koch
Methodology: Andrea Deiwick, Lothar Koch, Jordi Soriano
Supervision: Boris Chichkov
Visualization: Andrea Deiwick, Lothar Koch, Jordi Soriano
Writing – original draft: Lothar Koch, Andrea Deiwick, Jordi Soriano
Writing – review & editing: Lothar Koch, Andrea Deiwick, Jordi Soriano, Boris Chichkov

Ethics approval and consent to participate

Not applicable.

Consent for publication

Not applicable.

Availability of data

The data used in this study are available from the corresponding author upon reasonable request.

References

1. WHO, 2006, *Neurological Disorders: Public Health Challenges*, World Health Organization, Geneva, Switzerland, 204, table A.4.7.

2. Zhuang P, Sun AX, An J, *et al.*, 2018, 3D neural tissue models: From spheroids to bioprinting. *Biomaterials*, 154: 113–133.

   https://doi.org/10.1016/j.biomaterials.2017.10.002

3. Turunen S, Joki T, Hiltunen ML, *et al.*, 2017, Direct laser writing of tubular microtowers for 3D culture of human pluripotent stem cell-derived neuronal cells. *ACS Appl Mater Interfaces*, 9:25717–25730.

   https://doi.org/10.1021/acsami.7b05536

4. Cantley WL, Du C, Lomoio S, *et al*., 2018, Functional and sustainable 3D human neural network models from pluripotent stem cells. *ACS Biomater Sci Eng*, 4:4278–4288.

   https://doi.org/10.1021/acsbiomaterials.8b00622

5. Jakobsson A, Ottosson M, Zalis MC, *et al*., 2017, Three-dimensional functional human neuronal networks in uncompressed low-density electrospun fiber scaffolds. *Nanomed Nanotechnol Biol Med*, 13:1563–1573.

   https://doi.org/10.1016/j.nano.2016.12.023

6. Koroleva A, Deiwick A, El-Tamer A, *et al*., 2021, *In vitro* development of human iPSC-derived functional neuronal networks on laser-fabricated 3D scaffolds. *ACS Appl Mater Interfaces*, 13:7839–7853.

   https://doi.org/10.1021/acsami.0c16616

7. Lancaster MA, Renner M, Martin CA, *et al*., 2013, Cerebral organoids model human brain development and microcephaly. *Nature*, 501:373–379.

   https://doi.org/10.1038/nature12517

8. Camp JG, Badsha F, Florio M, *et al*., 2015, Human cerebral organoids recapitulate gene expression programs of fetal neocortex development. *Proc Natl Acad Sci USA*, 112:15672–15677.

   https://doi.org/10.1073/pnas.1520760112

9. Quadrato G, Brown J, Arlotta P, 2016, The promises and challenges of human brain organoids as models of neuropsychiatric disease. *Nat Med*, 22:1220–1228.

   https://doi.org/10.1038/nm.4214

10. Birey F, Andersen J, Makinson CD, *et al*., 2017, Assembly of functionally integrated human forebrain spheroids. *Nature*, 545:54–59.

    https://doi.org/10.1038/nature22330

11. Hofrichter M, Nimtz L, Tigges J, *et al*., 2017, Comparative performance analysis of human iPSC-derived and primary neural progenitor cells (NPC) grown as neurospheres *in vitro*. *Stem Cell Res*, 25:72–82.

    https://doi.org/10.1016/j.scr.2017.10.013

12. Takahashi K, Tanabe K, Ohnuki M, *et al*., 2007, Induction of pluripotent stem cells from adult human fibroblasts by defined factors. *Cell*, 131:861–872.

    https://doi.org/10.1016/j.cell.2007.11.019

13. Haase A, Olmer R, Schwanke K, *et al*., 2009, Generation of induced pluripotent stem cells from human cord blood. *Cell Stem Cell*, 5:434–441.

    https://doi.org/10.1016/j.stem.2009.08.021

14. Shi Y, Kirwan P, Livesey FJ, 2012, Directed differentiation of human pluripotent stem cells to cerebral cortex neurons and neural networks. *Nat Protoc*, 7:1836–1846.

    https://doi.org/10.1038/nprot.2012.116

15. Shi, Y, Inoue H, Wu JC, *et al*., 2017, Induced pluripotent stem cell technology: A decade of progress. *Nat Rev Drug Discov*, 16:115–130.

    https://doi.org/10.1038/nrd.2016.245

16. Canfield SG, Stebbins MJ, Faubion MG, *et al*., 2019, An isogenic neurovascular unit model comprised of human induced pluripotent stem cell-derived brain microvascular endothelial cells, pericytes, astrocytes, and neurons. *Fluids Barriers CNS*, 16:1–12.

    https://doi.org/10.1186/s12987-019-0145-6

17. Marton RM, Miura Y, Sloan SA, *et al*., 2019, Differentiation and maturation of oligodendrocytes in human three-dimensional neural cultures. *Nat Neurosci*, 22:484–491.

    https://doi.org/10.1038/s41593-018-0316-9

18. Xu T, Gregory CA, Molnar P, *et al*., 2006, Viability and electrophysiology of neural cell structures generated by the inkjet printing method. *Biomaterials*, 27:3580–3588.

    https://doi.org/10.1016/j.biomaterials.2006.01.048

19. Lee W, Pinckney J, Lee V, *et al*., 2009, Three-dimensional bioprinting of rat embryonic neural cells. *NeuroReport*, 20:798–803.

    https://doi.org/10.1097/WNR.0b013e32832b8be4

20. Lorber B, Hsiao WK, Hutchings IM, *et al*., 2014, Adult rat retinal ganglion cells and glia can be printed by piezoelectric inkjet printing. *Biofabrication*, 6:015001.

    https://doi.org/10.1088/1758-5082/6/1/015001

21. Lozano R, Stevens L, Thompson BC, *et al*., 2015, 3D printing of layered brain-like structures using peptide modified gellan gum substrates. *Biomaterials*, 67:264–273.

    https://doi.org/10.1016/j.biomaterials.2015.07.022

22. Kador KE, Venugopalan P, Malek MF, *et al*., 2016, Control of retinal ganglion cell positioning and neurite growth: Combining 3D printing with radial electrospun scaffolds. *Tissue Eng Part A*, 22:286–294.

    https://doi.org/10.1089/ten.TEA.2015.0373

23. Curley JL, Sklare SC, Bowser DA, *et al*., 2016, Isolated node engineering of neuronal systems using laser direct write. *Biofabrication*, 8:015013.

    https://doi.org/10.1088/1758-5090/8/1/015013

24. Song Y, Su X, Firouzian KF, *et al*., 2020, Engineering of brain-like tissue constructs via 3D cell-printing technology, *Biofabrication*, 12:035016.

    https://doi.org/10.1088/1758-5090/ab7d76

25. Roversi K, Ebrahimi Orimi H, Falchetti M, *et al*., 2021, Bioprinting of adult dorsal root ganglion (DRG) neurons using laser-induced side transfer (LIST). *Micromachines*, 12, 865.

    https://doi.org/10.3390/mi12080865

26. Lee, YB, Polio S, Lee W, *et al*., 2010, Bio-printing of collagen and VEGF-releasing fibrin gel scaffolds for neural stem cell culture. *Exp Neurol*, 223:645–652.

    https://doi.org/10.1016/j.expneurol.2010.02.014

27. Hsieh FY, Lin HH, Hsu SH, 2015, 3D bioprinting of neural stem cell-laden thermoresponsive biodegradable polyurethane hydrogel and potential in central nervous system repair. *Biomaterials*, 71:48–57.

    https://doi.org/10.1016/j.biomaterials.2015.08.028

28. Joung D, Truong V, Neitzke CC, *et al*., 2018, 3D printed stem-cell derived neural progenitors generate spinal cord scaffolds. *Adv Funct Mater*, 28:1801850.

    https://doi.org/10.1002/adfm.201801850

29. De la Vega L, Rosas Gómez AD, Abelseth E, *et al*., 2018, 3D bioprinting human induced pluripotent stem cell-derived neural tissues using a novel lab-on-a-printer technology. Appl Sci, 8:2414.

    https://doi.org/10.3390/app8122414

30. Salaris F, Colosi C, Brighi C, *et al*., 2019, 3D bioprinted human cortical neural constructs derived from induced pluripotent stem cells. *J Clin Med*, 8:1595.

    https://doi.org/10.3390/jcm8101595

31. Fantini V, Bordoni M, Scocozza F, et al 2019, Bioink composition and printing parameters for 3D modeling neural tissue. *Cells*, 8:830.

    https://doi.org/10.3390/cells8080830

32. Sharma R, Smits IPM, De La Vega L, *et al*., 2020, 3D bioprinting pluripotent stem cell derived neural tissues using a novel fibrin bioink containing drug releasing microspheres. *Front Bioeng Biotechnol*, 8:57.

    https://doi.org/10.3389/fbioe.2020.00057

33. Zhou L, Wolfes AC, Li Y, *et al*., 2020, 3D lipid-bilayer-supported 3D printing of human cerebral cortex cells reveals developmental interactions. *Adv Mater*, 32:e2002183.

    https://doi.org/10.1002/adma.202002183

34. Gu Q, Tomaskovic-Crook E, Wallace GG, *et al*., 2017, 3D bioprinting human induced pluripotent stem cell constructs for in situ cell proliferation and successive multilineage differentiation. *Adv Healthcare Mater*, 6:1700175.

    https://doi.org/10.1002/adhm.201700175

35. Gu Q, Tomaskovic-Crook E, Lozano R, *et al*., 2016, Functional 3D neural mini-tissues from printed gel-based bioink and human neural stem cells. *Adv Healthcare Mater*, 5:1429–1438.

    https://doi.org/10.1002/adhm.201600095

36. England S, Rajaram A, Schreyer DJ, *et al*., 2017, Bioprinted fibrin-factor XIII-hyaluronate hydrogel scaffolds with encapsulated Schwann cells and their in vitro characterization for use in nerve regeneration. *Bioprinting*, 5:1–9.

    https://doi.org/10.1016/j.bprint.2016.12.001

37. Ning L, Sun H, Lelong T, *et al*., 2018, 3D bioprinting of scaffolds with living Schwann cells for potential nerve tissue engineering applications. *Biofabrication*, 10:035014.

    https://doi.org/10.1088/1758-5090/aacd30

38. Li X, Wang X, Wang X, *et al*., 2018, 3D bioprinted rat Schwann cell-laden structures with shape flexibility and enhanced nerve growth factor expression. *Biotech*, 8:342.

    https://doi.org/10.1007/s13205-018-1341-9

39. Haring AP, Thompson EG, Tong Y, *et al*., 2019, Process- and bio-inspired hydrogels for 3D bioprinting of soft free-standing neural and glial tissues. *Biofabrication*, 11:025009.

    https://doi.org/10.1088/1758-5090/ab02c9

40. Wu Z, Li Q, Xie S, *et al*., 2020, *In vitro* and *in vivo* biocompatibility evaluation of a 3D bioprinted gelatin-sodium alginate/rat Schwann-cell scaffold. *Mater Sci Eng C Mater Biol Appl*, 109:110530.

    https://doi.org/10.1016/j.msec.2019.110530

41. Tse C, Whiteley R, Yu T, *et al*., 2016, Inkjet printing Schwann cells and neuronal analogue NG108-15 cells. *Biofabrication*, 8:015017.

    https://doi.org/10.1088/1758-5090/8/1/015017

42. Patz TM, Doraiswamy A, Narayan RJ, *et al*., 2006, Three-dimensional direct writing of B35 neuronal cells. *J Biomed Mater Res B*, 78:124–130.

    https://doi.org/10.1002/jbm.b.30473

43. Antill-O'Brien N, Bourke J, O'Connell CD, 2019, Layer-by-layer: The case for 3D bioprinting neurons to create patient-specific epilepsy models. *Materials*, 12:3218.

    https://doi.org/10.3390/ma12193218

44. Salaris F, Rosa A, 2019, Construction of 3D in vitro models by bioprinting human pluripotent stem cells: Challenges and opportunities. *Brain Res*, 1723:146393.

    https://doi.org/10.1016/j.brainres.2019.146393

45. Koch L, Deiwick A, Franke A, *et al*., 2018, Laser bioprinting of human induced pluripotent stem cells—The effect of printing and biomaterials on cell survival, pluripotency, and differentiation. *Biofabrication*, 10:035005.

    https://doi.org/10.1088/1758-5090/aab981

46. Koch L, Brandt O, Deiwick A, *et al*., 2016, Laser-assisted bioprinting at different wavelengths and pulse durations with a metal dynamic release layer: A parametric study. *Int J Bioprint*, 3:42–53.

    https://doi.org/10.18063/IJB.2017.01.001

47. Unger C, Gruene M, Koch L, *et al*., 2011, Time-resolved imaging of hydrogel printing via laser-induced forward transfer. *Appl Phys A*, 103:271–277.

https://doi.org/10.1007/s00339-010-6030-4

48. Gruene M, Deiwick A, Koch L, *et al*., 2011, Laser printing of stem cells for biofabrication of scaffold-free autologous grafts. *Tissue Eng Part C Methods*, 17:79.

https://doi.org/10.1089/ten.tec.2010.0359

49. Orlandi JG, Fernández-García S, Comella-Bolla A, *et al*., 2017, NETCAL: An interactive platform for large-scale, NETwork and population dynamics analysis of CALcium imaging recordings (Version 7.0.0 Open Beta), Zenodo.

https://doi.org/10.5281/ZENODO.1119026

50. Lütcke H, Gerhard F, Zenke F, *et al*., 2013, Inference of neuronal network spike dynamics and topology from calcium imaging data. *Front Neural Circuits*, 7:201.

https://doi.org/10.3389/fncir.2013.00201

51. Ludl AA, Soriano J, 2020, Impact of physical obstacles on the structural and effective connectivity of *in silico* neuronal circuits. *Front Comput Neurosci*, 14:77.

https://doi.org/10.3389/fncom.2020.00077

52. Stetter O, Battaglia D, Soriano J, *et al*., 2012, Model-free reconstruction of excitatory neuronal connectivity from calcium imaging signals. *PLoS Comput Biol*, 8:e1002653.

https://doi.org/10.1371/journal.pcbi.1002653

53. Orlandi JG, Stetter O, Soriano J, *et al*., 2014, Transfer entropy reconstruction and labeling of neuronal connections from simulated calcium imaging. *PLoS One*, 9:e98842.

https://doi.org/10.1371/journal.pone.0098842

54. Tibau E, Ludl AA, Rudiger S, *et al*., 2020, Neuronal spatial arrangement shapes effective connectivity traits of in vitro cortical networks. *IEEE Trans Netw Sci Eng*, 7:435–448.

https://doi.org/10.1109/TNSE.2018.2862919

55. Rubinov M, Sporns O, 2010, Complex network measures of brain connectivity: uses and interpretations. *Neuroimage*, 52:1059–1069.

https://doi.org/10.1016/j.neuroimage.2009.10.003

56. Latora V, Marchiori M, 2001, Efficient behavior of small-world networks. *Phys Rev Lett*, 87:198701.

https://doi.org/10.1103/PhysRevLett.87.198701

57. Blondel VD, Guillaume JL, Lambiotte R, *et al*., 2009, Fast unfolding pf communities in large networks. *J Stat Mech*, P10008:1–12.

https://doi.org/10.1088/1742-5468/2008/10/P10008

58. Knight VB, Serrano EE, 2017, Post-translational tubulin modifications in human astrocyte cultures. *Neurochem Res*, 42(9):2566–2576.

https://doi.org/10.1007/s11064-017-2290-0

59. Verwer RW, Sluiter AA, Balesar RA, *et al*., 2007, Mature astrocytes in the adult human neocortex express the early neuronal marker doublecortin. *Brain*, 130(Pt 12):3321–3335.

https://doi.org/10.1093/brain/awm264

60. Sahara S, Yanagawa Y, O'Leary DDM, *et al*., 2012, The fraction of cortical GABAergic neurons is constant from near the start of cortical neurogenesis to adulthood. *J Neurosci*, 32:4755–4761.

https://doi.org/10.1523/JNEUROSCI.6412-11.2012

61. Hanada T, 2020, Ionotropic glutamate receptors in epilepsy: A review focusing on AMPA and NMDA receptors. Biomolecules, 10:464.

https://doi.org/10.3390/biom10030464

62. Berridge MJ, Lipp P, Bootman MD, 2000, The versatility and universality of calcium signaling. *Nat Rev Mol Cell Biol*, 1:11–21.

https://doi.org/10.1038/35036035

63. Grienberger C, Konnerth A, 2012, Imaging calcium in neurons. *Neuron*, 73:862.

https://doi.org/10.1016/j.neuron.2012.02.011

64. Klapper SD, Garg P, Dagar S, *et al*., 2019, Astrocyte lineage cells are essential for functional neuronal differentiation and synapse maturation in human iPSC-derived neural networks. *Glia*, 67:1893–1909.

https://doi.org/10.1002/glia.23666

65. Farhy-Tselnicker I, Allen NJ, 2018, Astrocytes, neurons, synapses: A tripartite view on cortical circuit development. *Neural Dev*, 13:7.

https://doi.org/10.1186/s13064-018-0104-y